


Discovery and Characterization of *R/S-N-3-Cyanophenyl-N'-(6-tert-butoxycarbonylamino-3,4-dihydro-2,2-dimethyl-2H-1-benzopyran-4-yl)urea*, a New Histone Deacetylase Class III Inhibitor Exerting Antiproliferative Activity against Cancer Cell Lines

Michael Schneckenger,†,◆ Eric Goffin,‡,◆ Jin-Young Lee,§ Jun Young Jang,§ Aloran Mazumder,§ Seungwon Ji,§ Bernard Rogister,|| Nafila Bouider,‡ Florence Lefranc,⊥ Walter Miklos,# Véronique Mathieu,○ Pascal de Tullio,‡ Kyu-Won Kim,▽ Mario Dicato,† Walter Berger,# Byung Woo Han,§ Robert Kiss,○ Bernard Pirotte,*‡,|| and Marc Diederich*,§,||

†Laboratoire de Biologie Moléculaire et Cellulaire du Cancer, Hôpital Kirchberg, 9, Rue Edward Steichen, L-2540 Luxembourg, Luxembourg

‡Laboratory of Medicinal Chemistry, Center for Interdisciplinary Research on Medicines (CIRM), University of Liège, 4000 Liège, Belgium

§Department of Pharmacy, Research Institute of Pharmaceutical Sciences, College of Pharmacy, Seoul National University, 1 Gwanak-ro, Gwanak-gu, Seoul 151-742, Korea

||Nervous System Diseases and Treatment, GIGA-Neurosciences, University of Liège, 4000 Liège, Belgium

⊥Service de Neurochirurgie, Hôpital Erasme, Université Libre de Bruxelles, 1070 Brussels, Belgium

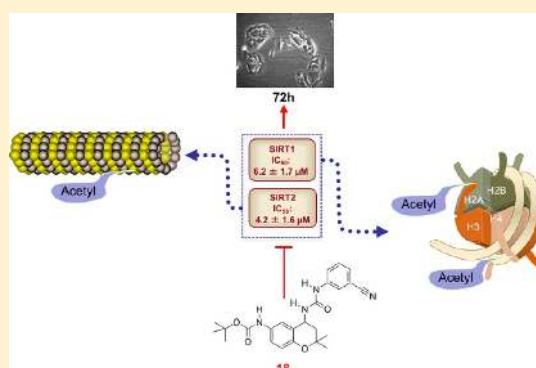
#Department of Medicine I, Comprehensive Cancer Center and Institute of Cancer Research, Medical University of Vienna, 1090 Vienna, Austria

▽SNU-Harvard Neurovascular Protection Center, College of Pharmacy and Research Institute of Pharmaceutical Sciences, Seoul National University, Seoul 151-742, Korea

○Laboratoire de Cancérologie et de Toxicologie Expérimentale, Faculté de Pharmacie, Université Libre de Bruxelles, 1050 Brussels, Belgium

Supporting Information

ABSTRACT: A new series of *N*-aryl-*N'*-3,4-dihydro-2,2-dimethyl-2*H*-1-benzopyran-4-yl)ureas bearing an alkoxy carbonylamino group at the 6-position were synthesized and examined as putative anticancer agents targeting sirtuins in glioma cells. On the basis of computational docking combined to in vitro sirtuin 1/2 inhibition assays, we selected compound **18** [*R/S-N-3-cyanophenyl-N'-(6-tert-butoxycarbonylamino-3,4-dihydro-2,2-dimethyl-2H-1-benzopyran-4-yl)urea*] which displays a potent antiproliferative activity on various glioma cell types, assessed by quantitative videomicroscopy, eventually triggering senescence. The impact on normal glial cells was lower with a selectivity index of >10. Furthermore, human U373 and Hs683 glioblastoma cell lines served to demonstrate the inhibitory activity of **18** against histone deacetylase (HDAC) class III sirtuins 1 and 2 (SIRT1/2) by quantifying acetylation levels of histone and non-histone proteins. The translational potential of **18** was validated by an NCI-60 cell line screen and validation of growth inhibition of drug resistant cancer cell models. Eventually, the anticancer potential of **18** was validated in 3D glioblastoma spheroids and in vivo by zebrafish xenografts. In summary, compound **18** is the first representative of a new class of SIRT inhibitors opening new perspectives in the medicinal chemistry of HDAC inhibitors.



■ INTRODUCTION

Glioblastomas are associated with dismal prognoses due to their intrinsic resistance to proapoptotic stimuli,¹ and temozolomide, a generic compound, remains today the most efficient chemotherapeutic agent to fight glioblastoma once maximal surgery and radiotherapy have already been performed.² Considering the absence of chemotherapeutically active drugs against

glioblastoma, the reduced life expectancy of the patients, and the specific molecular characteristics of this type of cancer, it becomes increasingly clear that new compound groups and molecular targets need to be investigated. Recently, histone

Received: April 6, 2017

Published: May 5, 2017

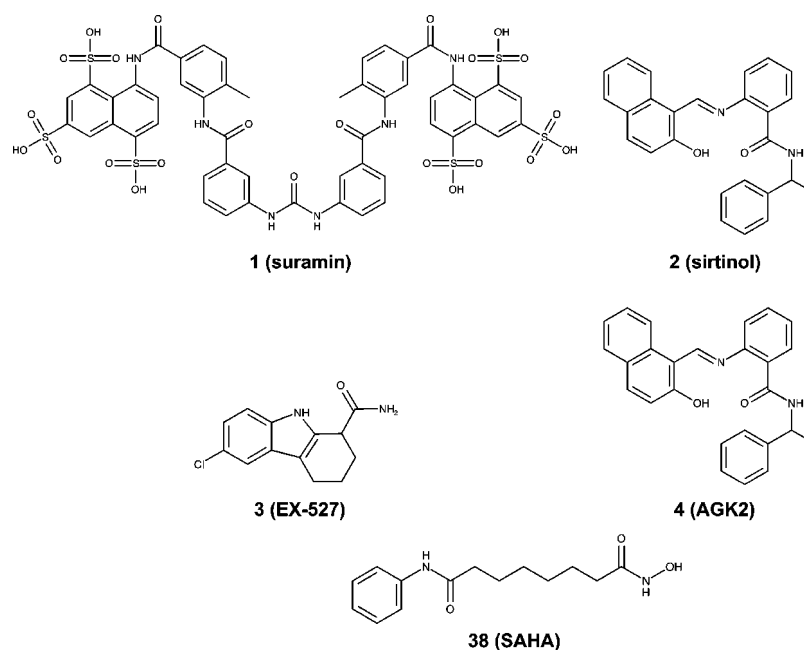


Figure 1. Reference HDAC inhibitors.

deacetylase (HDAC) and sirtuin (SIRT) inhibitors (SIRTi) were shown to trigger metabolic effects in glioblastoma independently or combined with temozolomide,³ allowing speculation about the potential impact of SIRTi on this cancer type.

NAD⁺-dependent deacetylase class III of HDACs comprises a family of seven members, namely, SIRT1–7, known to deacetylate histones and other target proteins. Intracellular localization characterizes the different isoforms (SIRT1/2, nucleus or cytoplasm; SIRT3–5, mitochondria; SIRT6, nucleus; SIRT7, nucleolus) as well as substrate specificity: besides histones, many transcriptional regulators and mitochondrial proteins are deacetylated by SIRTs.^{4,5}

SIRTs are emerging targets for the treatment of various chronic diseases including cancer.^{6,7} Especially, both SIRT1 and -2 have been reported to play a key role in the development of cancer.^{8,9} Accordingly, first inhibitors comprised compounds resembling the physiological substrates such as NAD⁺ analogs that were described as competitive SIRTi compounds that compete with NAD⁺ for the NAD⁺-binding domain, thus inhibiting enzymatic activity of multiple SIRTs. Such compounds showed anticancer activity in B-cell chronic lymphoblastic leukemia or prostate cancer.¹⁰ Suramin (1) (Figure 1), an adenosine receptor antagonist, acts as a SIRTi by binding the C pocket, B pocket, and partially the enzyme's substrate-binding site.¹¹ 1 was shown to possess anticancer potential in combination with cytotoxic agents in xenografted prostate, lung, and breast cancer cells.¹² Similarly, sirtinol (2) (Figure 1), a well described SIRT1 and -2 selective inhibitor, displays anticancer properties against various cancer models.^{9,10} Although, most SIRTi compounds lack selectivity against a specific isoform, EX-527 (3) (Figure 1) was reported to inhibit SIRT1 but is less active against SIRT2 and SIRT3.¹³ A combination treatment using 3 and other HDAC inhibitors was found to induce apoptosis in acute myeloid leukemia cells.¹⁰ The selective inhibition of SIRT2 by AGK2 (4) (Figure 1)¹⁴ has been reported to induce anticancer effects by suppressing tumor cell growth and migration.¹⁵

Recently, some of our structural analogs of the ATP-sensitive potassium (K_{ATP}) channel opener cromakalim (5), 6-halo-substituted

3,4-dihydro-2,2-dimethyl-2H-1-benzopyrans (or 2,2-dimethylchromans), bearing an arylurea or arylthiourea moiety at the 4-position (6: X = F, Cl, Br), were described as potent inhibitors of glioma. Here we synthesized a series of *N*-aryl-*N'*-3,4-dihydro-2,2-dimethyl-2H-1-benzopyran-4-yl)ureas and thioureas bearing an alkoxy-carbonylamino group ("carbamate" group) at the 6-position (6: X = NHCOOR) and investigated their anticancer effects on glial tumor cells (Figure 2). Our results show that compound 18

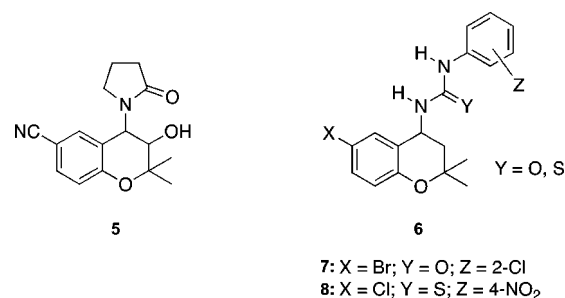


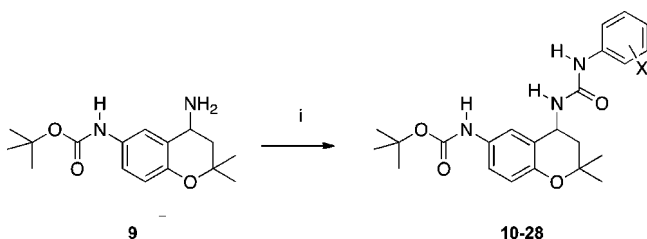
Figure 2. Chemical structure of cromakalim (5) and general formula of 4-aryleura/arylthiourea-substituted 2,2-dimethylchromans (6) previously reported as K_{ATP} channel openers. Compounds 7 and 8 are examples of 2,2-dimethylchromans exerting antiproliferative activity against glioma cell lines.

[*R/S-N*-3-cyanophenyl-*N'*-(6-*tert*-butoxycarbonylamino-3,4-dihydro-2,2-dimethyl-2H-1-benzopyran-4-yl)urea] inhibits SIRT1/2 activity associated with a potent antiproliferative activity on glioblastoma cells while having a lower impact on normal glial cells, thus demonstrating an excellent differential toxicity. For the first time, we document here the *in vitro* characterization of 18 as a novel SIRT inhibitor and its in cellulo epigenetic effect combined with its anticancer potential in 2D and 3D cell culture. Our results are validated *in vivo* by zebrafish glioblastoma xenografts.

RESULTS AND DISCUSSION

Chemistry. The synthesis of the key intermediate 9 has been previously described.¹⁶ The target compounds 10–28 were

prepared in good yields by reaction of **9** with the appropriate monosubstituted phenyl isocyanate in methylene chloride at room temperature (Scheme 1).

Scheme 1^a

^aReagents: (i) X-C₆H₄-N=C=O, CH₂Cl₂, rt, 75–85%.

Starting from the *N*-3-cyanophenyl-substituted urea **18**, the corresponding *N*-3-aminomethyl-substituted analog **22** was obtained after reduction of the cyano group using hydrogen gas in the presence of Raney nickel⁰ (Scheme 2). On the other hand, acid-catalyzed deprotection of the *tert*-butyl carbamate group of **18** provided the corresponding 6-amino-substituted chroman **33**, which by formylation gave access to the 6-formamido-substituted analog **34** (Scheme 2).

Reduction of the nitro group of compound **19** into the amino-substituted compound **23** was performed with iron powder in the presence of ammonium chloride in ethanol/water 3:1 (Scheme 3).

The target compound **32** was obtained by reaction of the previously described compound **31**¹⁷ with 3-cyanophenyl isocyanate (Scheme 4).

All the compounds were crystallized from appropriate solvents and characterized by ¹H and ¹³C NMR. Their purity was assessed by elemental analysis to obtain the final materials with the chemical purity required before pharmacological evaluations.

Growth Inhibitory Activity against Glioma Cells. The *in vitro* effects of the 2,2-dimethylchromans **10–28** and **32–37** on the growth of three human high-grade glioma cell lines, i.e., U373 and T98G from astroglial origin and Hs683 from

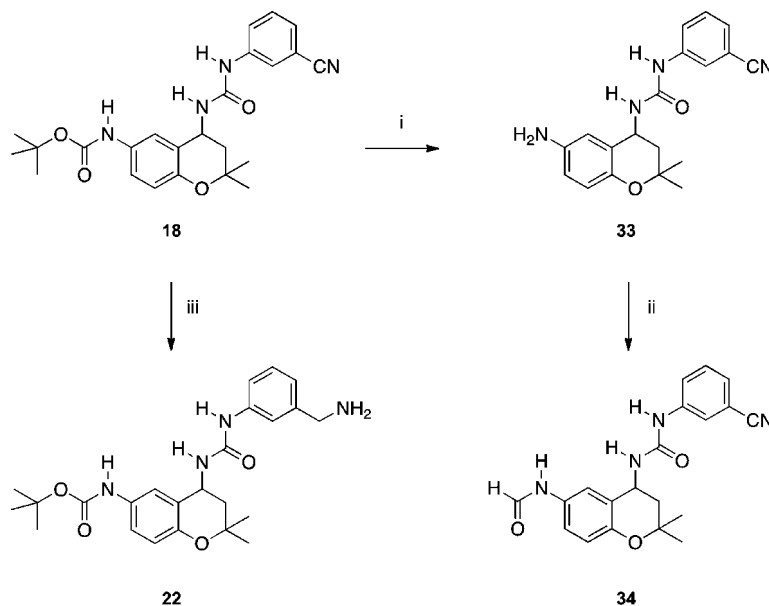
oligodendroglial origin, were examined (Tables 1 and 2; see Experimental Section for details). Moreover, the selective toxicity between normal astrocytes and glioma cells regarding *in vitro* growth inhibition was also investigated for several compounds listed in Table 1.

The 2,2-dimethylchroman compounds tested on glioma cells were characterized by the presence of a variety of substituents at the ortho, meta, or para position of the phenyl ring in the arylurea or arylthiourea moiety located at the 4-position of the benzopyran ring. The monosubstitution was investigated in these three positions with moderate to strong electron withdrawing (halogen, CN, NO₂, CF₃) or electron donating (OCH₃, NH₂) groups (Table 1). With a second set of compounds, the nature of the substituent in the 6-position was also examined (Table 2). Particular attention was paid to the progressive increase of the steric hindrance of the “carbamate” moiety in this position.

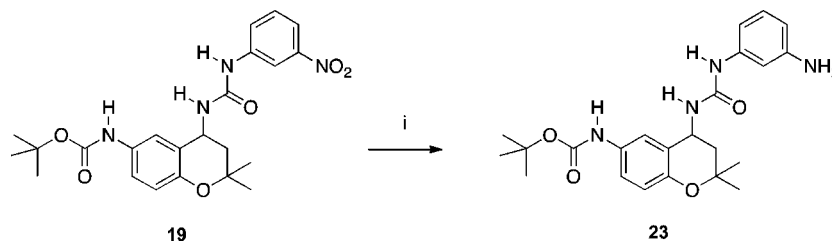
From the data reported in Table 1, it was observed that for the compounds bearing the same substituent on the phenyl ring, the ortho position was generally found to be less favorable for growth inhibitory activity on glioma cells than the meta and the para positions (compare **10** versus **16** and **24**; compare **11** versus **18** and **25**; compare **13** versus **20** and **27**). However, no general trend can be formally deduced. The nitro group, for example, was better tolerated in the ortho position than in the para position, while the meta position remains the best choice for improved activity against all tumor cell lines (see **12**, **19**, and **26**).

It also appears that for growth inhibitory activity on glioma cells, an electron withdrawing group was preferred to an electron donating group (i.e., positive mesomeric effect of OCH₃ and NH₂), in particular in the meta and the para positions (compare **21** and **23** versus **15–20**; compare **28** versus **24–27**).

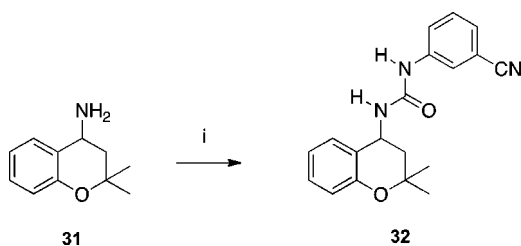
Taken as a whole, the two best compounds from Table 1 were the 3-cyano and the 3-nitro-substituted arylurea compounds **18** and **19**, with an equal potency compared to cisplatin in these three tumor cell lines models, and 4-cyano-substituted arylthiourea compound **30**, previously described as an inhibitor of insulin release.¹⁶ Interestingly, the reduction of the cyano

Scheme 2^a

^aReagents: (i) 5 N HCl in EtOH, rt, 80% ; (ii) HCOOH, Ac₂O, THF, rt, 80–85%; (iii) H₂, Raney nickel⁰, EtOH, 65%.

Scheme 3^a

^aReagents: (i) Fe, NH₄Cl, EtOH, H₂O, 50%.

Scheme 4^a

^aReagents: (i) 3-cyanophenyl isocyanate, CH₂Cl₂, rt, 90–95%.

group of **18**, which provides the corresponding aminomethyl-substituted derivative **22**, gave rise to a complete loss of biological activity.

Results reported in Table 2 clearly indicated that the presence of a bulky *tert*-butoxycarbonylamino group (see **18**) was preferred to less bulky “carbamate” moieties (see **35**, **36**, **37**) or the absence of a substituent (see **32**). The introduction of an amino (**33**) or a formamido group (**34**) was responsible for a complete loss of growth inhibitory activity against the three tumor cell lines.

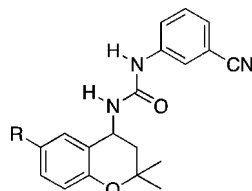
Finally, looking at the selectivity index defined as the ratio between the GI₅₀ values on normal and tumor astrocytes, **18**

Table 1. In Vitro Growth Inhibitory Activity against Three Human Glioma Cell Lines and Determination of Cell Selectivity Using Murine Normal Astrocytes (Modulation of the 4-Position)

compd	Y	R	in vitro IC ₅₀ (μM) ^{a,d}			mean ^d	Sel ^{b,d}	AclogP ^c
			U373	T98G	Hs683			
10	O	2-Cl	59 ± 11	88 ± 24	34 ± 3	60 ± 27	-	4.65
11	O	2-CN	45 ± 8	67 ± 7	54 ± 5	55 ± 11	-	3.99
12	O	2-NO ₂	12 ± 1	22 ± 2	13 ± 1	16 ± 6	>10	4.20
13	O	2-CF ₃	>100	-	-	-	-	4.86
14	O	2-OCH ₃	30 ± 1	39 ± 1	59 ± 4	43 ± 15	-	3.96
15	O	3-F	20 ± 1	26 ± 1	19 ± 2	22 ± 4	-	4.23
16 ^e	O	3-Cl	18 ± 2	20 ± 3	12 ± 3	17 ± 4	>12	4.65
17	O	3-Br	22 ± 1	26 ± 3	18 ± 1	22 ± 4	-	4.79
18 ^e	O	3-CN	6 ± 1	14 ± 1	4 ± 1	8 ± 5	>10	3.85
19	O	3-NO ₂	1 ± 1	7 ± 4	16 ± 2	8 ± 8	<5	4.04
20	O	3-CF ₃	9 ± 1	21 ± 2	9 ± 1	13 ± 7	<2	4.86
21	O	3-OCH ₃	30 ± 1	>100	37 ± 2	>56	-	3.97
22	O	3-CH ₂ NH ₂	>100	>100	95 ± 4	>98	-	3.10
23	O	3-NH ₂	97 ± 2	>100	91 ± 5	>96	-	3.24
24 ^e	O	4-Cl	22 ± 1	26 ± 3	26 ± 3	25 ± 2	-	4.65
25 ^e	O	4-CN	10 ± 1	26 ± 1	18 ± 2	18 ± 8	>10	3.85
26	O	4-NO ₂	24 ± 1	26 ± 1	20 ± 1	23 ± 3	-	4.05
27	O	4-CF ₃	10 ± 1	15 ± 2	11 ± 1	12 ± 3	>10	4.86
28	O	4-OCH ₃	33 ± 1	49 ± 2	62 ± 9	48 ± 15	-	3.24
29 ^e	S	3-CN	19 ± 3	10 ± 2	26 ± 2	18 ± 8	<2	4.28
30 ^e	S	4-CN	7 ± 1	7 ± 1	7 ± 1	7 ± 1	-	4.28
cisplatin	NA ^f	NA ^f	4 ± 1	12 ± 4	4 ± 1	7 ± 3	NA ^f	NA ^f

^aIC₅₀ values: concentration of drug responsible for the inhibition of 50% of the growth of the specified cell line after 72 h [mean ± SEM (*n* = 6 replicates)]. ^b“Sel” means the level of selectivity, i.e., IC₅₀ values obtained on murine normal astrocytes (*n* = 3)/IC₅₀ values obtained on human tumor astrocytes (*n* = 3). ^cAclogP: calculated log *P* values according to the ALOGPS 2.1 software [VCCLAB, Virtual Computational Chemistry Laboratory, <http://www.vcclab.org>, 2005]. ^d“–” = not determined. ^ePublished compounds in refs **16** and **56**. ^fNA: not applicable.

Table 2. In Vitro Growth Inhibitory Activity against Three Human Glioma Cell Lines (Modulation of the 6-Position)



compd	R	in vitro IC ₅₀ (μM) ^a			mean	AclogP ^b
		U373	T98G	Hs683		
32	H	38 ± 2	32 ± 5	31 ± 5	34 ± 3	2.52
33	NH ₂	>100	>100	>100	>100	2.52
34	NHCHO	>100	>100	>100	>100	2.41
35 ^c	NHCOOCH ₃	45 ± 10	56 ± 7	84 ± 8	60 ± 20	2.82
36 ^c	NHCOC ₂ H ₅	38 ± 2	46 ± 4	15 ± 2	33 ± 16	3.19
37 ^c	NHCOOCH(CH ₃) ₂	8 ± 1	40 ± 5	45 ± 6	31 ± 20	3.53
18 ^c	NHCOOC(CH ₃) ₃	6 ± 1	14 ± 1	4 ± 1	8 ± 5	3.85

^aIC₅₀ values: concentration of drug responsible for the inhibition of 50% of the growth of the specified cell line after 72 h [mean ± SEM (*n* = 6 replicates)]. ^bAclogP: calculated log *P* values according to the ALOGPS 2.1 software [VCCLAB, Virtual Computational Chemistry Laboratory, <http://www.vcclab.org>, 2005]. ^cPublished compounds in ref 56.

(with a selectivity index of >10) was identified as one of the most promising compounds.

Biology. Therapeutic Potential of SIRT1 and -2 Targeting in Glioblastoma. Since the simultaneous inhibition of SIRT1 and -2 has been shown to display promising anticancer properties,^{8,18} we aimed to assess the therapeutic potential of the pharmacological targeting of SIRT1 and -2 in glioblastoma. First, we investigated basal SIRT1 and -2 protein expression levels in U373 and Hs683 (Figure 3A). Results showed that Hs683 cells expressed a high constitutive level of SIRT1 compared to U373 cell, whereas SIRT2 was expressed at higher levels in U373 cells. Accordingly, we then knocked down SIRT1 in Hs683 and SIRT1 and SIRT2 in U373 using siRNAs (Figure 3B) and followed their effects on cell growth (Figure 3C) by videomicroscopy over 72 h. Results suggested that a depletion of SIRT1 or -2 strongly reduced the proliferation of glioblastoma cells, thus further validating SIRT1 and -2 as interesting pharmacological targets.

Predicting SIRT1/2 Binding Affinity of 2,2-Dimethylchroman Derivatives. To combine the differential cytotoxicity of our 2,2-dimethylchromans to their potential to inhibit SIRT1/2 activities, we compared the binding affinity of selected 2,2-dimethylchroman derivatives to known SIRTi including 2 as a dual SIRT1/2 inhibitor, 3 (SIRT1 inhibitor), and 4 (SIRT2 inhibitor). First, derivatives were analyzed against the human SIRT1 complex [Protein Data Bank (PDB) code 4I5I] and SIRT2 complex (PDB code 4RMG) using AutoDock Vina¹⁹ as described in “Experimental Section”. Briefly, the SIRT1 and -2 complexes were divided into ligand and protein and then the ligands were docked into the protein complexes. In silico docking results are represented in Table 3 and Figure SI-1 in Supporting Information.

Since compound 18 with the *N*-alkyl-*N'*-arylurea group in its *cis*, *trans* low-energy conformation demonstrated best docking affinity against SIRT1/2 (Figure 4), a qualitative molecular docking was then performed with compound 18 in comparison to the SIRTi 4 and 2 against seven available experimental cocrystallized human SIRT2 complexes. The resulting lowest binding affinities were compared (Table 4A).^{20–23} Overall, compound 18 exhibited a similar affinity to 2 but less than 4. In Figure 4A, the lowest affinity pose of compound 18 was selected as the likely

binding modes in the binding pocket of SIRT2 (PDB code 4RMG) where compound 18 formed a hydrogen bond with the backbone carbonyl oxygen of Val233. In addition, similar docking experiments were performed using compound 18 in comparison with the SIRTi 3 and 2 against six available experimental cocrystallized human SIRT1 complexes (Table 4B).^{24–27} Compound 18 exhibited better binding affinities than 3 and 2. The lowest binding affinity pose of compound 18 was selected as the likely binding mode in the binding pocket of SIRT1 protein (PDB code 4I5I) where compound 18 formed two hydrogen bonds with the backbone nitrogen of Ala262 and the Nδ atom of His363 (Figure 4B).

Compound 18 Acts as a SIRT1/2 Inhibitor. Considering the proficiency of various HDAC inhibitors to impair glioblastoma cell proliferation^{3,28} and the strong effect of the depletion of SIRT1 and -2 on glioblastoma cell growth, we then validated the potential of various 2,2-dimethylchromans selected based on our computational docking results to inhibit SIRT activities in vitro (Table 5). In agreement with our docking data, compound 18 markedly inhibited both SIRT1 (IC₅₀ = 6.2 ± 1.7 μM) and SIRT2 (IC₅₀ = 4.2 ± 1.6 μM) activities within a concentration range comparable to 1 used as a positive control, even though 1 showed higher selectivity for SIRT1 (2.8 ± 0.3 μM) versus SIRT2 (13 ± 1 μM), whereas other derivatives performed less well or not at all.

Collectively, these data pointed out compound 18 as a good drug candidate for further investigation. First, we evaluated the selectivity of 18 by testing its activity against total in vitro HDAC activities (Figure 5A) as well as against the in vitro activity of various nonsirtuin HDAC isoenzymes (Figure 5B). Results showed only residual inhibition of total HDAC activity, whereas increasing concentrations (0.1–100 μM) of 18 did not significantly impact HDAC 1, 2, 3, 8, 6, 10, and 11 activities. Therefore, compound 18 appeared essentially as a potent inhibitor of SIRT1/2 but not of SIRT3. Presently, we cannot exclude that 18 also targets other SIRT isoforms insofar expressed by glioblastoma.

To validate in vitro results, 18 was then investigated on human U373 and Hs683 glioblastoma to assess in cellulo effects of SIRT inhibition on acetylation levels of histone and non-histone proteins. Cells were treated for 24 h at concentrations of 1–10 μM

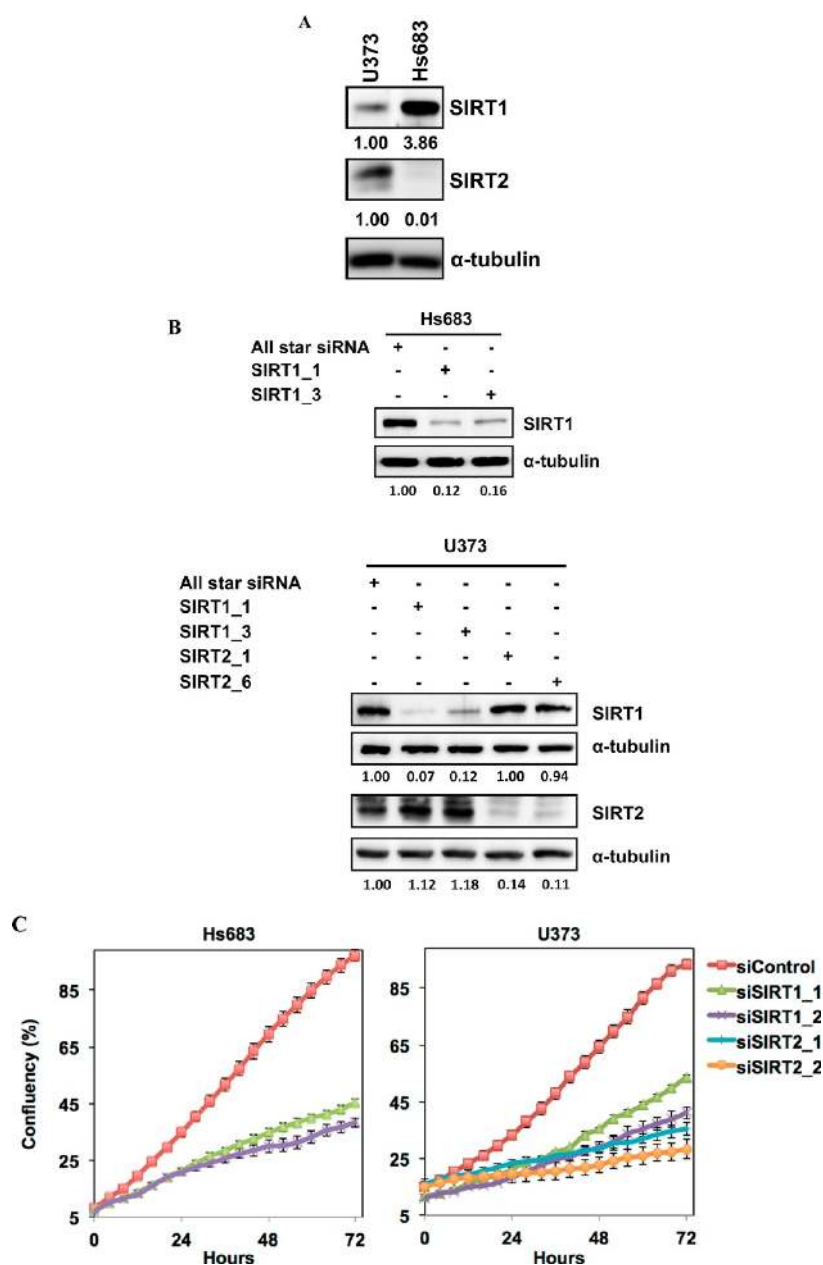


Figure 3. SIRT1/2 silencing decreases glioblastoma cell proliferation. (A) Constitutive SIRT1 and SIRT2 protein expression levels in U373 and Hs683 cell lines analyzed by Western blot. α -Tubulin was used as a loading control. (B, C) U373 and Hs683 cell lines were transfected with the indicated siRNA. (B) SIRT1 and SIRT2 protein expression levels were analyzed 24 h post-transfection. β -Actin was used as loading control. (C) 24 h post-transfection cell proliferation was monitored by time-lapse videomicroscopy. Graphs are representative of three independent experiments and correspond to the mean \pm SD of 16 pictures per well acquired in triplicate. Blots are representative of three independent experiments, and quantifications are indicated under the blots.

18 compared to the pan-HDAC inhibitor suberoylanilide hydroxamic acid (SAHA, **38**; 2 μ M) used as a positive control (Figures 1 and 6). We observed a concentration-dependent increase of α -tubulin, a well-known protein substrate for SIRT2,²⁹ and histone H4 acetylation starting at 5 μ M in U373 cells and 1–2.5 μ M in Hs683 cells, respectively. The differential dose–response of protein acetylation observed in those two cell lines after **18** exposure depending on the analyzed sirtuin substrate could be explained by the constitutive SIRT1 and -2 protein expression levels observed in glioblastoma cell lines (Figure 3A). Furthermore, **18** increased acetylation levels in both lines for acetylated H4 and H3K56, reported to serve as substrates for SIRT1 (Figure SI-2).

Furthermore, we compared the growth inhibitory activity of **18** to reference SIRTi against U373 and Hs683 cell lines (Table 6). MTT results highlighted **18** as a promising anticancer drug as it had the most pronounced growth inhibitory potency against glioblastoma cells, about 6 times compared to the SIRT1/2 inhibitor **2** and about 20 and 6–14 times for the SIRT1 and SIRT2 inhibitors **3** and **4**, respectively.

Finally, we investigated the effect of the depletion of SIRT1 or SIRT2 on the anticancer effects of compound **18** in glioblastoma cells. Results demonstrated that the downregulation of either one of these two HDAC enhanced the growth inhibitory properties of compound **18** on U373 and Hs683 cells (Figure 7).

Table 3. In Silico Docking Scores of Selected Compounds against Human SIRT1 and SIRT2^a

compd	SIRT1, PDB code 4ISI	SIRT2, PDB code 4RMG
2	-7.0	-8.7
3	-9.4	-
4	-	-11.3
8	-8.3	-8.6
10	-9.2	-10.0
11	-8.4	-9.6
12	-7.5	-8.8
16	-7.6	-9.6
18	-11.1	-10.0
19	-7.2	-8.2
24	-7.2	-9.5
25	-7.7	-9.0
29	-7.6	-9.3
30	-7.8	-9.6
35	-9.0	-9.6
36	-8.2	-9.2
37	-10.7	-10.6

^aBinding affinity energy values (kcal/mol) for the indicated PDB codes were calculated using AutoDock Vina (for more details see Experimental Section). 2, 3, and 4 were used as reference inhibitors of SIRT1/2, SIRT1, and SIRT2, respectively. "-" = not determined.

Compound 18 Does Not Exert Its Growth Inhibitory Activity through Proapoptotic Effects in Human Glioblastoma Cells. We then assessed the biological effect of compound 18 by using computer-assisted phase contrast microscopy (quantitative videomicroscopy) to grossly analyze the way by which compound 18 inhibits the growth of human U373 and Hs683 glioma cell lines (Figure 8). Figure 8A shows that 10 μ M (i.e., approximately the GI₅₀ value revealed by the MTT colorimetric assay, Table 1) compound 18 decreased by ~70% the growth of the Hs683 cell line after 72 h of culture. While the growth inhibitory effects of 18 were pronounced on Hs683 cell line growth, the 18-related growth inhibitory activity rather corresponded to cytostatic than to cytotoxic effects on these Hs683 tumor cells as morphologically illustrated in Figure 8. The definitions of the global growth and the global growth ratio are provided in the legend of Figure 8. The same features were observed on the U373 glioblastoma cells (Figure 8B). Remarkably, while U373 glioblastoma cells display certain levels of resistance to proapoptotic stimuli,³⁰ these U373 cells appear as sensitive as Hs683 oligodendroglioma cells to the growth inhibitory effects of compound 18 (Table 1, Figure 8) with the fact that Hs683 cells are sensitive to proapoptotic stimuli.^{30,31}

The quantitative videomicroscopy-related analyses suggested that compound 18 is cytostatic rather than cytotoxic in both Hs683 and U373 glioma cell lines. We thus made use of flow cytometry analyses to investigate whether compound 18 induced, or not, significant proapoptotic effects in these two glioma cell lines. The data obtained with 10 μ M compound 18 indicated modest proapoptotic effects in Hs683 and weak, if any, effects in U373 glioma cells (Figure SI-3). It is thus unlikely that the growth inhibitory effects observed at 10 μ M for compound 18 (Table 1, Figure 8) could relate to cytotoxic proapoptotic effects, even if, as expected,^{30,31} Hs683 oligodendroglioma cells are more prone to enter apoptosis than U373 glioblastoma cells. Indeed, while both the MTT colorimetric assay and the quantitative videomicroscopy approach revealed that 10 μ M compound 18 inhibited by \geq 50% the growth of both Hs683 and

U373 glioma cell lines (Table 1, Figure 8), flow cytometry analyses revealed that 10 μ M compound 18 induced ~25% and <10% apoptosis in Hs683 and U373 glioma cells, respectively (Figure SI-3). These results were confirmed and generalized by the absence of a significant accumulation of cells in the sub G1 population (Figure SI-4) when cells were treated with various SIRTi at the IC₅₀ calculated from MTT assays (Table 6). Only 4 induced a modest increase of sub G1 population in both cell lines as observed with the pan-non-sirtuin HDAC inhibitor 38 in U373 cells.

Effect of Compound 18 on Cell Cycle and Senescence.

Considering the strong effect of 18 on glioblastoma cell growth, we then investigated the effect of various SIRTi compounds on cell cycle distribution. As shown in Figure 9A, compound 18 induced an accumulation in G1 in both cell lines comparable to the one observed with the SIRT1 inhibitor 3 as well as with the SIRT1/2 inhibitor 2 and the pan-non-sirtuin inhibitor 38 in Hs683 cells. In contrast, the SIRT2 inhibitor 4 triggered G2/M accumulation in both cell lines as observed with 2 and 38 in U373 cells.

Irreversible cell cycle arrest may result in senescence induction.³² Therefore, we investigated whether sustained exposure to subtoxic concentrations of compound 18 may promote senescence-associated β -galactosidase (SA- β -gal) activity. As shown in Figure 9B, the number of senescent cells, identified as blue-stained cells, was markedly increased in 18-treated U373 cells (\cong 20%), whereas no blue-stained cells were detected in untreated cells.

Compound 18 Inhibits Glioblastoma Cell Growth in Vivo. Considering the drastic antiproliferative properties of 18 in vitro, we next investigated whether this compound could also hamper the spheroid-forming capacity of glioblastoma cells. Our results show that 5 and 10 μ M compound 18 significantly reduced the surface area and volume of multicellular tumor spheroids from glioma Hs683 (Figure 10A) and U373 (Figure SI-5) cell lines. The propensity of compound 18 to reduce the 3D tumor-like growth of glioblastoma cells was also confirmed by decreased ATP levels in 18-treated tumor spheroid glioblastoma cultures (Figures 10A and SI-5).

To further extend our evaluation of the growth inhibitory capacities of 18 toward in vivo settings, we examined the ability of 18 to abrogate tumor development in a zebrafish xenotransplantation model. Fluorescently labeled tumor cells were pre-treated for 30 (Figure SI-5) or 36 h (Figure 10B) with compound 18 and then injected into the yolk sacs of zebrafish embryos. Results revealed that the tumor-associated fluorescence intensity signal was drastically lowered in the 18-treated zebrafish group compared to the untreated control group for both glioblastoma Hs683 and U373 cell lines. The capacity of 18 to impede tumor formation in vivo validated our in vitro results and sustained the potential anticancer activity of 18.

Compound 18 Is Active against a Broad Range of Tumor Cell Lines Including Drug-Resistant Cancer Cells Harboring Different Resistance Mechanisms. Next, to extend the anticancer potential of 18, Figure 11 (revealed with the permission of the NCI) shows that the mean GI₅₀ value of compound 18 in the NCI-60 cell line panel is log₁₀ GI₅₀ = -5.52, i.e., ~3 μ M, a concentration very close to the one we obtained on the three Hs683, U373, and T98G glioma cell lines, i.e., 8 \pm 5 μ M (Table 1). Figure 11 further shows that compound 18 displays similar growth inhibitory activity against a broad majority of the NCI cell lines.

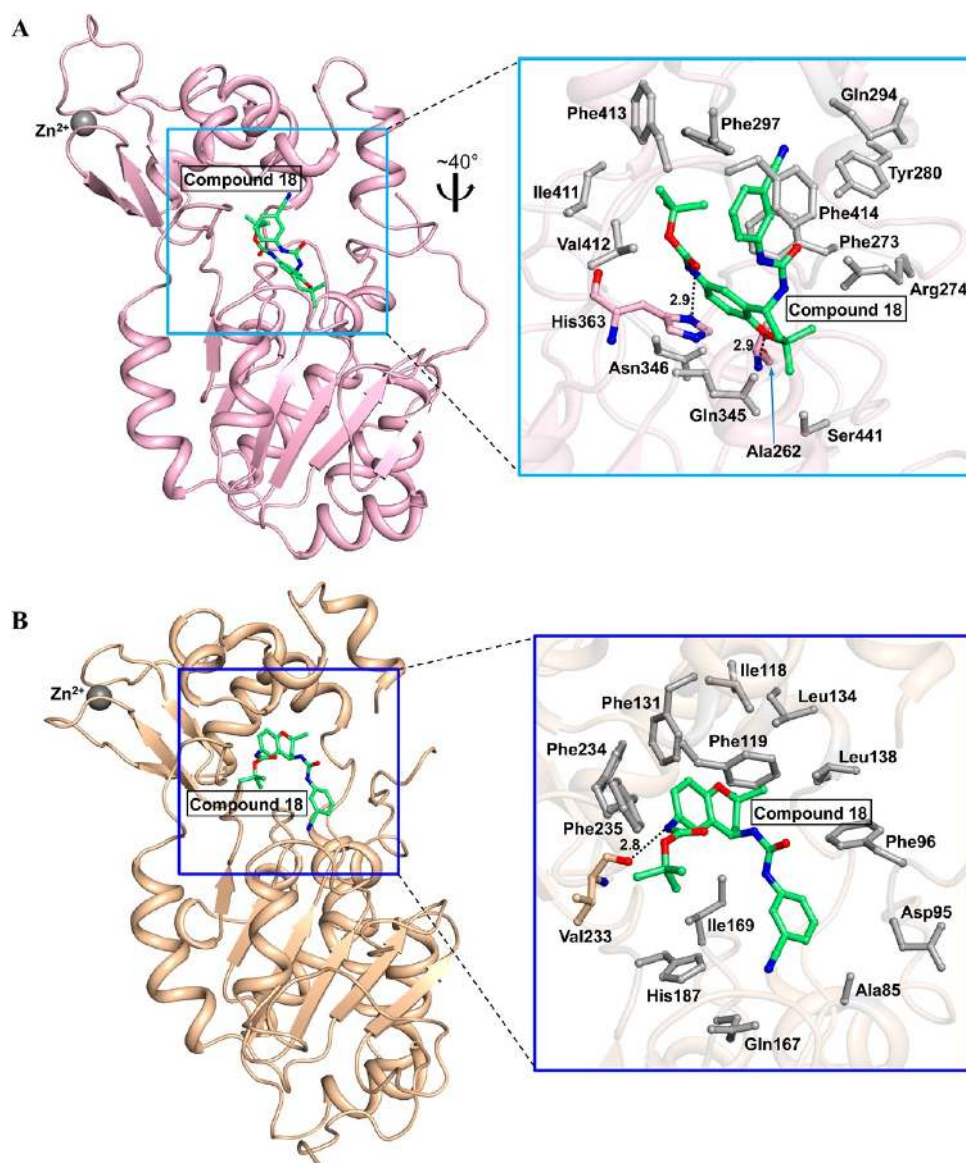


Figure 4. Compound **18** docked into human SIRT1 and SIRT2. (A) Docking pose of compound **18** on the crystal structure of SIRT1 (light pink; PDB code 4I5I). Close-up view on the right shows that compound **18** (lime) binds to the active site of SIRT1 structure. Hydrogen bonds are shown as dashed black lines. The residues forming hydrophobic interactions are represented as gray colored sticks. (B) Docking pose of compound **18** on the crystal structure of SIRT2 (wheat; PDB code 4RMG). Close-up view on the right shows that compound **18** (lime) binds to the active site of SIRT2 structure. The hydrogen bond is shown as dashed black lines. The residues forming hydrophobic interactions are represented as gray colored sticks.

Successful cancer therapy by chemotherapeutic agents but also targeted small molecule inhibitors is frequently limited by drug resistance mechanisms leading to treatment failure and recurrence. Resistance might be mediated by mutations in sensor genes of DNA damage, like the tumor suppressor p53³³ or overexpression of pleiotropic efflux pumps for multiple drugs causing a broad-scale multidrug resistance (MDR) phenotype.³⁴ Hence we tested whether mutation of p53 or overexpression of the major MDR proteins ABCB1 (P-glycoprotein) and ABCC1 (multidrug resistance protein 1, MRP1) significantly reduces the anticancer activity of **18** (Figure 12). Neither loss of p53 nor overexpression of these ABC transporters resulted in a significant loss of activity against the investigated drug resistance models (Table SI-1). In contrast, ABCB1 overexpression in SW1573 2R160 and KB-C-1 lines even resulted in a slight hypersensitivity to **18** (Figure 12B and Figure 12D, respectively, and Table SI-1). Additionally, an ovarian cancer cell model with acquired cisplatin

resistance (A2780cis) and a hydroxyurea-resistant HeLa derivative overexpressing ribonucleotide reductase model (KB-HU)³⁵ were compared to their respective parental cell lines (Figure 12C and Figure 12D, respectively). Also in these two cases, no significant impact of the resistance phenotype on the cytotoxic activity of **18** was detectable. Collectively these data demonstrate that **18** is not susceptible to several important chemotherapy resistance mechanisms.

Finally, the effect of **18** was tested after 24 and 48 h of treatment on the viability of peripheral blood mononuclear cells (PBMCs) from healthy donors (Figure 13). Compound **18** does not exhibit any major acute toxicity on this normal cell model.

CONCLUSIONS

We prepared new series of *N*-aryl-*N'*-3,4-dihydro-2,2-dimethyl-2*H*-1-benzopyran-4-yl)ureas and thioureas bearing an alkoxy-carbonylamino group ("carbamate" group) at the 6-position of the

Table 4. Qualitative Molecular Docking of Compound 18 against Human SIRT1 (A) and SIRT2 (B)^a

(A)			
SIRT1 PDB code	18	2	3
4I5I	-11.1	-7.0	-9.4
4IG9	-8.5	-8.8	-7.3
4ZZH	-8.5	-8.4	-7.5
4ZZI	-9.9	-9.9	-8.7
4ZZJ	-7.4	-9.8	-8.8
5BTR	-8.4	-7.9	-6.8
average	-9.0	-8.6	-8.1
(B)			
SIRT2 PDB code	18	2	4
4RMG	-10.0	-8.7	-11.3
4RMH	-10.6	-8.8	-11.5
1J8F	-7.5	-9.8	-9.3
3ZGO	-8.1	-10.3	-9.1
3ZGV	-9.1	-9.8	-8.7
5DY4	-9.4	-11.0	-10.6
5DYS	-9.5	-7.5	-9.8
average	-9.2	-9.4	-10.0

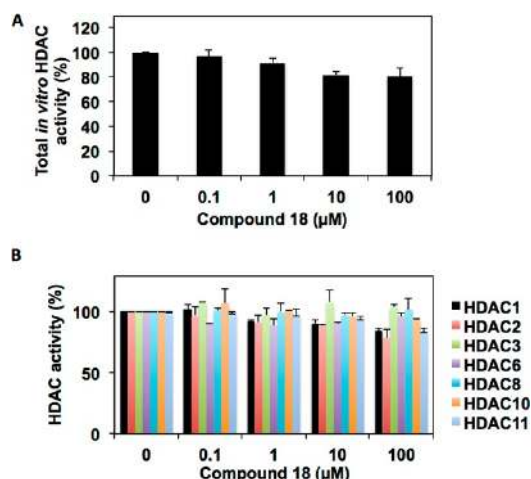
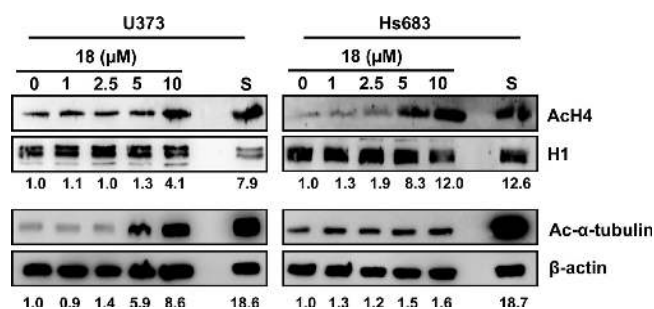
^aBinding affinity energy values (kcal/mol) for the indicated PDB codes were calculated using AutoDock Vina program (for more details see Experimental Section). 2, 3, and 4 were used as reference inhibitors of SIRT1/2, SIRT1, and SIRT2, respectively.

Table 5. Inhibitory Activity of Selected SIRT Inhibitors and Compound 18 on SIRT1, -2, and -3 Activities

compd	IC ₅₀ (μM) ^a		
	SIRT1	SIRT2	SIRT3
1	2.8 ± 0.3	13 ± 1	>200
2	82.5 ± 7.1	47.1 ± 4.0	-
3	0.10 ± 0.06	20.1 ± 4.2	-
4	98.1 ± 2.4	2.8 ± 1.0	-
8	>200	>200	-
16	32.1 ± 6.5	18.5 ± 3.6	-
18	6.2 ± 1.7	4.2 ± 1.6	>200
19	>200	99.8 ± 11.0	-
25	121.2 ± 18.3	110.2 ± 18.9	-
35	109.9 ± 6.1	49.4 ± 7.6	-
36	108.7 ± 5.9	51.1 ± 11.1	-
37	54.8 ± 8.3	22.7 ± 3.5	-

^aIC₅₀ values: concentration of drug required for the inhibition of 50% of the specified sirtuin activity [mean ± SD (*n* = 3 independent experiments)]. 1 and 2, 3, and 4 were used as in vitro reference inhibitors of SIRT1/2, SIRT1, and SIRT2, respectively. "-": not determined.

chroman nucleus. These compounds, structurally related to previously described 2,2-dimethylchroman derivatives acting on glioma cells, were examined as putative anticancer agents. Growth inhibitory activity was measured in three glioma cell lines (U373, T98G, and Hs683), as well as on normal astrocytes. Those data revealed that the compound bearing a cyano group at the meta position of the phenyl ring of the 4-arylurea moiety, as well as a bulky *tert*-butoxycarbonylamino group at the 6-position (compound 18), exhibited a potent antiproliferative activity against the tumor glial cells while having lower impact on normal glial cells (selectivity index of >10). From the computational docking analysis, compound 18 also showed a potent binding affinity when compared with other derivatives as observed with

**Figure 5.** In vitro HDAC inhibition potential of compound 18. (A) Residual inhibition of total HDAC activity. (B) Effect of 18 on activity of selected HDAC isoenzymes. Data are the mean ± SD of three independent experiments.**Figure 6.** In cellulo assessment of HDAC inhibition by compound 18 through the study of histone and α -tubulin acetylation levels. Cells were treated for 8 h at the indicated concentrations of compound 18. The acetylation (Ac) of histone H4 (H4) and α -tubulin was analyzed by Western blot. Histone H1 (H1) and β -actin were used as loading controls for the analysis of acid (top panel) and total (bottom panel) extracts, respectively. 38 (2 μ M) was used as a reference HDAC inhibitor.**Table 6. Growth Inhibitory Activities of Selected SIRT Inhibitors and Compound 18 in Glioma Cell Lines**

compd	IC ₅₀ (μM) ^a	
	U373	Hs683
2	39.3 ± 5.4	33.9 ± 4.3
3	157.4 ± 23.0	115.9 ± 23.3
4	47.6 ± 4.4	80.2 ± 9.3
18	7.5 ± 1.1	5.8 ± 0.9

^aIC₅₀ values: concentration of drug responsible for the inhibition of 50% of the growth of the specified cell line after 72 h [mean ± SEM of three independent experiments (*n* = 4 replicates)].

our antiproliferative activity assay. This compound was therefore selected for further investigations to better understand its mechanism of action. Compound 18 was assayed in the NCI-60 cell line panel screening demonstrating interesting inhibitory potential in various cell types. 18 was also submitted to a COMPARE analysis (results not presented) to further decipher the mode of action of compound 18 as successfully done previously with respect to other compounds but without providing further clues. The screening confirmed the antiproliferative

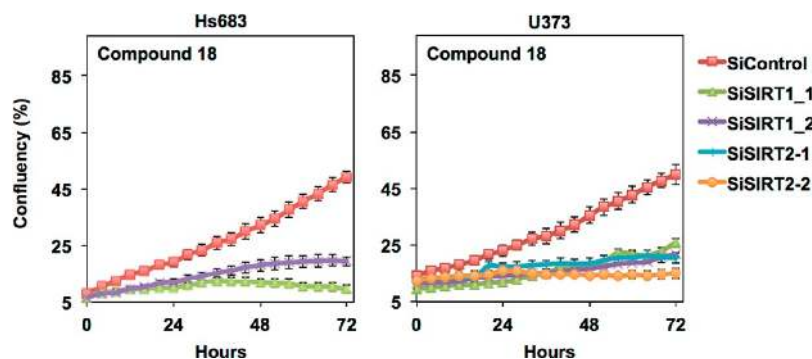


Figure 7. SIRT1 or SIRT2 knock-down enhances the growth inhibitory effects of **18** in glioblastoma cells. U373 and Hs683 cell lines were transfected with the indicated siRNA. 24 h post-transfection cells were treated with compound **18** at the respective IC_{50} values calculated from MTT assays (Table 6), and proliferation was monitored by time-lapse videomicroscopy. Graphs are representative of three independent experiments and correspond to the mean \pm SD of 16 pictures per well acquired in triplicate.

activity of **18** on a variety of cancer cell lines (mean GI_{50} value of $3 \mu M$), while the COMPARE tool did not allow obtaining a clear hypothesis about its potential mechanism of action. Quantitative videomicroscopy analysis revealed that **18** was a cytostatic rather than a cytotoxic agent.

Furthermore, neither mutation of p53 nor overexpression of MDR efflux pumps including ABCB1 and ABCC1 significantly reduced the anticancer activity of **18**. The same holds true for acquired cisplatin and hydroxyurea resistance. These data suggest that several major drug resistance mechanisms limiting the success of current systemic cancer therapy are not affecting the activity of **18**. Hence this substance might be especially attractive for targeting treatment-resistant recurrences.

Then, **18** was tested against a panel of HDAC activities and a potent inhibitory activity was observed in vitro on HDAC SIRT1/2 and IC_{50} values in the low micromolar range (Table 3). Presently, we cannot exclude that inhibition of other SIRT isoforms led to growth arrest if expressed by the targeted cancer type. This observation was validated in cellulo when **18** was investigated on human U373 and Hs683 glioblastoma cell lines to assess effects of deacetylase inhibition on acetylation levels of histone and non-histone proteins. Interestingly, compound **18** acted as an in vitro SIRTi with activities commonly reported in the literature. Importantly we demonstrated associated biological activities (i.e., increased protein acetylation levels and important antiproliferative properties) at concentrations in the low micromolar range, which is usually not the case of SIRTi published over the past years (Table SI-4).

Finally, the anticancer potential of **18** was further highlighted through the growth inhibition of multicellular glioblastoma tumor spheroids as well as the reduction of tumor formation in vivo using zebrafish xenografts.

In conclusion, compound **18** is new anticancer agent active on glioma cells and expressing a cytostatic rather than a cytotoxic activity. Moreover, this compound is a potent inhibitor of SIRT1 and -2 and constitutes a model of chemical structure opening new perspectives in the medicinal chemistry of HDAC inhibitors against class III.

EXPERIMENTAL SECTION

Chemistry. Melting points were determined on a Stuart SMP3 capillary apparatus and are uncorrected. The 1H NMR spectra were recorded on a Bruker Avance (500 MHz) instrument using $DMSO-d_6$ as the solvent with TMS as an internal standard; chemical shifts are reported in δ values (ppm) relative to that of internal TMS. The abbreviations s = singlet, d = doublet, t = triplet, q = quadruplet,

m = multiplet, b = broad are used throughout. Elemental analyses (C, H, N, S) were realized on a Thermo Scientific FlashEA 1112 elemental analyzer and were within $\pm 0.4\%$ of the theoretical values. This analytical method certified a purity of $\geq 95\%$ for each tested compound. All reactions were routinely checked by TLC on silica gel Merck 60 F_{254} .

R/S-N-2-Chlorophenyl-N'-(6-tert-butoxycarbonylamino-3,4-dihydro-2,2-dimethyl-2H-1-benzopyran-4-yl)urea (10). 3-Chlorophenyl isocyanate (0.13 g, 0.82 mmol) was added to a solution of **9** (0.2 g, 0.68 mmol) in methylene chloride (5 mL). After 1 h, the solvent was removed under vacuum; the title product was obtained from the crude product by DCVC purification: mp 192–194 °C; 1H NMR ($DMSO-d_6$) δ 1.25 (s, 3H, CH_3), 1.36 (s, 3H, CH_3), 1.43 (s, 9H, $NHCOOC(CH_3)_3$), 1.66 (dd, $J = 13$ Hz/11 Hz, 1H, 3-H), 2.13 (dd, $J = 13$ Hz/6 Hz, 3-H), 4.91 (dd, $J = 16$ Hz/9 Hz, 1H, 4-H), 6.65 (d, $J = 8.8$ Hz, 1H, 8-H), 6.97 (td, $J = 7.9$ Hz/1.5 Hz, 1H, 4'-H), 7.19 (d, $J = 7.1$ Hz, 1H, 7-H), 7.27 (td, $J = 7.9$ Hz/1.5 Hz, 1H, 5'-H), 7.38 (d, $J = 8.4$ Hz, 1H, $CHNHCONHAr$), 7.41–7.42 (m, 2H, 5-H/3'-H), 8.07 (s, 1H, $CHNHCONHAr$), 8.26 (dd, $J = 8.3$ Hz/1.2 Hz, 1H, 6'-H), 9.10 (s, 1H, $NHCOOC(CH_3)_3$). ^{13}C NMR ($DMSO-d_6$) δ 24.6 (CH_3), 28.1 ($C(CH_3)_3$), 28.9 (CH_3), 40.0 (C-3), 42.4 (C-4), 74.7 (C-2), 78.6 ($C(CH_3)_3$), 116.7 (C-8), 117.7 (C-5), 119.7 (C-7), 120.7 (C-6'), 121.1 (C-2'), 122.5 (C-4'), 122.6 (C-4a), 127.5 (C-5'), 129.1 (C-3'), 132.1 (C-6), 136.6 (C-1'), 148.6 (C-8a), 153.0 ($NHCOOC(CH_3)_3$), 154.7 ($CHNHCONHAr$). Anal. ($C_{23}H_{28}ClN_3O_4$) theoretical: C, 61.95; H, 6.33; N, 9.42. Found: C, 61.71; H, 6.33; N, 9.44.

R/S-N-2-Cyanophenyl-N'-(6-tert-butoxycarbonylamino-3,4-dihydro-2,2-dimethyl-2H-1-benzopyran-4-yl)urea (11). The title compound was obtained as described for **10**, starting from **9** (0.2 g, 0.68 mmol) and 2-cyanophenyl isocyanate (0.12 g, 0.82 mmol): mp 206–208 °C; 1H NMR ($DMSO-d_6$) δ 1.25 (s, 3H, CH_3), 1.36 (s, 3H, CH_3), 1.43 (s, 9H, $NHCOOC(CH_3)_3$), 1.69 (dd, $J = 13$ Hz/11 Hz, 1H, 3-H), 2.14 (dd, $J = 13$ Hz/6 Hz, 3-H), 4.91 (dd, $J = 16$ Hz/9 Hz, 1H, 4-H), 6.65 (d, $J = 8.8$ Hz, 1H, 8-H), 7.12 (t, $J = 8$ Hz, 1H, 4'-H), 7.20 (d, $J = 7.3$ Hz, 1H, 7-H), 7.42 (d, $J = 8.8$ Hz, 1H, $CHNHCONHAr$), 7.43 (s, 1H, 5-H), 7.61 (m, 1H, 5'-H), 7.71 (dd, $J = 7.8$ Hz/1.4 Hz, 3'-H), 8.22 (d, $J = 8.5$ Hz, 1H, 6'-H), 8.54 (s, 1H, $CHNHCONHAr$), 9.11 (s, 1H, $NHCOOC(CH_3)_3$). ^{13}C NMR ($DMSO-d_6$) δ 24.6 (CH_3), 28.1 ($C(CH_3)_3$), 28.8 (CH_3), 40.0 (C-3), 42.6 (C-4), 74.7 (C-2), 78.6 ($C(CH_3)_3$), 100.5 (C-2'), 116.8 (C-8), 117.0 (CN), 117.6 (C-5), 119.7 (C-7), 120.4 (C-6'), 122.2 (C-4'), 122.4 (C-4a), 132.1 (C-6), 133.0 (C-3'), 133.9 (C-5'), 142.7 (C-1'), 148.5 (C-8a), 153.0 ($NHCOOC(CH_3)_3$), 154.4 ($CHNHCONHAr$). Anal. ($C_{24}H_{28}N_4O_4$) theoretical: C, 66.04; H, 6.47; N, 12.84. Found: C, 66.12; H, 6.11; N, 13.26.

R/S-N-2-Nitrophenyl-N'-(6-tert-butoxycarbonylamino-3,4-dihydro-2,2-dimethyl-2H-1-benzopyran-4-yl)urea (12). The title compound was obtained as described for **10**, starting from **9** (0.2 g, 0.68 mmol) and 2-nitrophenyl isocyanate (0.13 g, 0.82 mmol): mp 218–219 °C; 1H NMR ($DMSO-d_6$) δ 1.25 (s, 3H, CH_3), 1.37 (s, 3H, CH_3), 1.42 (s, 9H, $NHCOOC(CH_3)_3$), 1.69 (dd, $J = 13$ Hz/11 Hz, 1H, 3-H), 2.11 (dd, $J = 13$ Hz/6 Hz, 3-H), 4.92 (dd, $J = 16$ Hz/9 Hz, 1H,

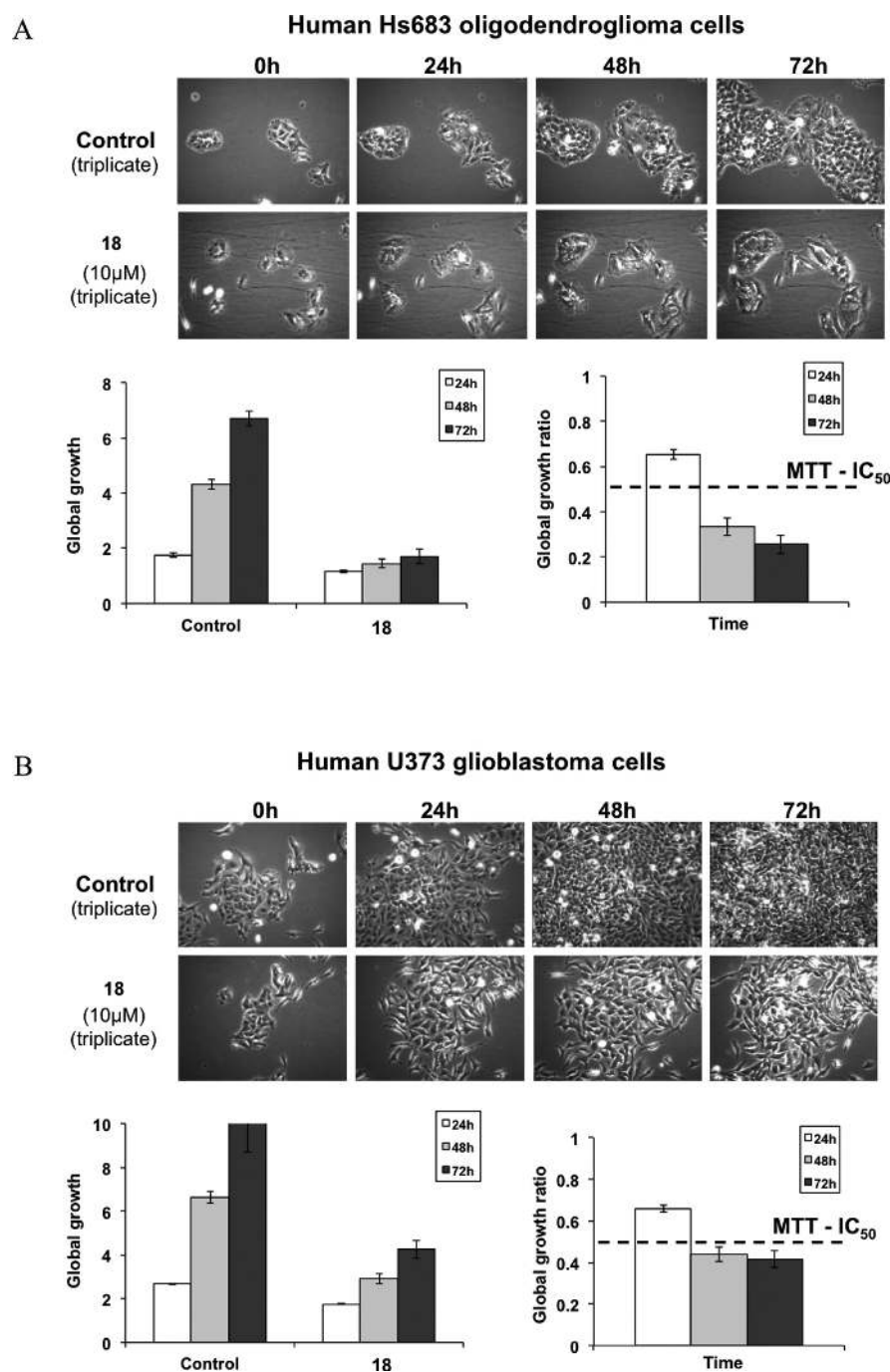


Figure 8. Digitized images of Hs683 oligodendroglial (A) and U373 glioblastoma (B) cells were obtained using computer-assisted phase-contrast microscopy (quantitative videomicroscopy). A global growth ratio (the GGR index) was calculated, resulting in a value that can be directly compared to the IC_{50} value determined by the MTT colorimetric assay (the hatched horizontal line in the bottom chart, i.e., $\sim 10 \mu M$ (see Table 1)). First, the global growth (GG) is calculated for each control and each treated condition at 24, 48, and 72 h by dividing the number of cells on the last image by the number of cells on the first image. The GGR index is obtained by dividing the GG values calculated for Hs683 tumor cells treated with 18 by the GG values calculated for the control. The experiment was performed once in triplicate, and the data represent the mean \pm SEM values. White, gray, and black bars represent the data obtained at 24, 48 and 72 h, respectively.

4-*H*), 6.65 (d, $J = 8.8$ Hz, 1H, 8-*H*), 7.16 (m, 1H, 4'-*H*), 7.20 (d, $J = 6.4$ Hz, 1H, 7-*H*), 7.40 (s, 1H, 5-*H*), 7.68 (m, 1H, 5'-*H*), 7.98 (d, $J = 8.1$ Hz, 1H, CHNHCONHAr), 8.09 (dd, $J = 8.4$ Hz/1.5 Hz, 1H, 6'-*H*), 8.45 (d, $J = 8.5$ Hz, 1H, 3'-*H*), 9.09 (s, 1H, NHCOOC(CH₃)₃), 9.45 (s, 1H, CHNHCONHAr). ¹³C NMR (DMSO-*d*₆) δ 24.4 (CH₃), 28.1 (C(CH₃)₃), 29.0 (CH₃), 40.0 (C-3), 42.7 (C-4), 74.7 (C-2), 78.6 (C(CH₃)₃), 116.7 (C-8), 117.7 (C-5), 119.6 (C-7), 121.5 (C-4'), 122.1 (C-3'), 122.4 (C-4a), 125.4 (C-6'), 132.0 (C-6), 135.0 (C-5'), 135.8 (C-1'), 136.7 (C-2'), 148.5 (C-8a), 152.9 (NHCOOC(CH₃)₃), 154.2

(CHNHCONHAr). Anal. (C₂₃H₂₈N₄O₆) theoretical: C, 60.52; H, 6.18; N, 12.27. Found: C, 60.18; H, 6.17; N, 11.86.

R/S-N-2-Trifluoromethylphenyl-N'-(6-tert-butoxycarbonylamino-3,4-dihydro-2,2-dimethyl-2H-1-benzopyran-4-yl)urea (13). The title compound was obtained as described for 10, starting from 9 (0.2 g, 0.68 mmol) and 2-trifluoromethylphenyl isocyanate (0.15 g, 0.82 mmol): mp 239–239.5 °C; ¹H NMR (DMSO-*d*₆) δ 1.25 (s, 3H, CH₃), 1.36 (s, 3H, CH₃), 1.44 (s, 9H, NHCOOC(CH₃)₃), 1.67 (dd, $J = 13$ Hz/11 Hz, 1H, 3-*H*), 2.12 (dd, $J = 13$ Hz/6 Hz, 3-*H*), 4.90

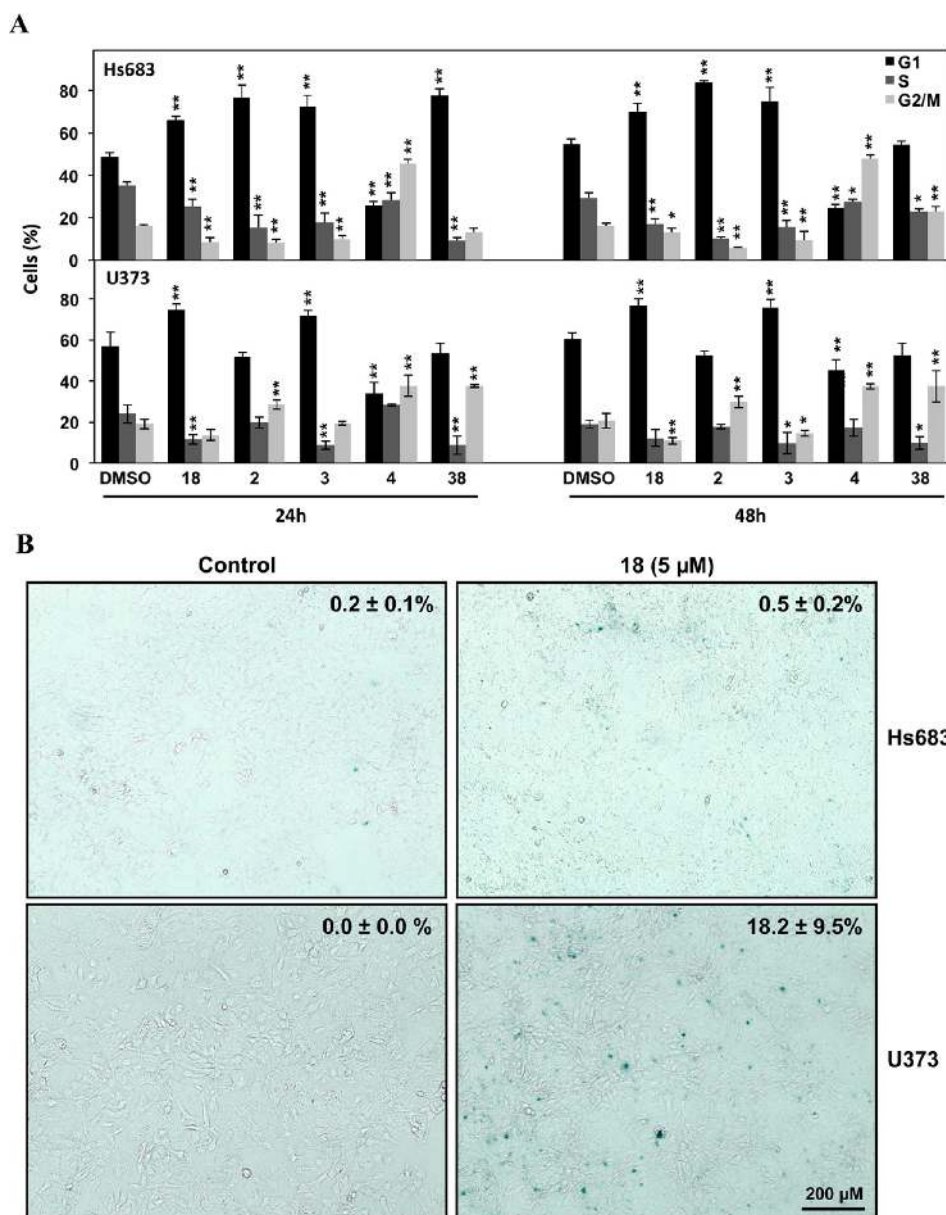


Figure 9. Compound 18 induces G1 cell cycle arrest in glioblastoma cell lines and promotes the accumulation of senescent U373 cells. (A) Cells were treated, or not, with 18, 2, 3, 4 (at the respective IC_{50} values for each cell lines reported in Table 6) and 2 μ M 38. After 24 and 48 h of exposure, cell cycle distribution was analyzed. Histograms correspond to the mean \pm SD of the quantification of three independent experiments. *, ** indicate $p < 0.05$, $p < 0.01$ compared to control cells, respectively. (B) Cells were incubated in a medium containing DMSO as a vehicle control or 5 μ M 18 for 6 days and were stained for β -galactosidase activity. Representative pictures of two independent experiments are depicted where SA- β -gal-positive cells are revealed by blue staining. The percentage of senescent cells, expressed as a percentage of the total number of cells counted, is indicated for each picture. Data represent the mean \pm SD of two independent experiments.

(dd, $J = 16$ Hz/9 Hz, 1H, 4-H), 6.64 (d, $J = 8.8$ Hz, 8-H), 7.15 (d, $J = 7.6$ Hz, 1H, 7-H), 7.21 (t, $J = 7.6$ Hz, 1H, 4'-H), 7.38 (d, $J = 8.3$ Hz, 1H, CHNHCONHAr), 7.48 (s, 1H, 5-H), 7.60 (t, $J = 7.8$ Hz, 1H, 5'-H), 7.63 (d, $J = 7.9$ Hz, 1H, 3'-H), 7.83 (s, 1H, CHNHCONHAr), 8.09 (d, $J = 8.3$ Hz, 1H, 6'-H), 9.12 (s, 1H, NHCOOC(CH₃)₃). ¹³C NMR (DMSO-*d*₆) δ 24.6 (CH₃), 28.1 (C(CH₃)₃), 28.9 (CH₃), 40.0 (C-3), 42.6 (C-4), 74.7 (C-2), 78.6 (C(CH₃)₃), 116.7 (C-8), 117.8 (C-5), 119.6 (C-7), 122.7 (C-4a), 122.8 (C-4'), 123.0–125.1 (d, $J = 273$ Hz, CF₃), 124.8 (C-6'), 125.7 (C-3'), 127.3 (C-2'), 132.0 (C-6), 132.7 (C-5'), 137.2 (C-1'), 148.5 (C-8a), 152.9 (NHCOOC(CH₃)₃), 154.9 (CHNHCONHAr). Anal. (C₂₄H₂₈F₃N₃O₄) theoretical: C, 60.12; H, 5.89; N, 8.76. Found: C, 60.12; H, 5.95; N, 8.73.

R/S-N-2-Methoxyphenyl-N'-(6-tert-butoxycarbonylamino-3,4-dihydro-2,2-dimethyl-2H-1-benzopyran-4-yl)urea (14). The title compound was obtained as described for 10, starting from 9

(0.2 g, 0.68 mmol) and 2-methoxyphenyl isocyanate (0.12 g, 0.82 mmol): mp 204–205 °C; ¹H NMR (DMSO-*d*₆) δ 1.25 (s, 3H, CH₃), 1.35 (s, 3H, CH₃), 1.42 (s, 9H, NHCOOC(CH₃)₃), 1.62 (dd, $J = 13$ Hz/11 Hz, 1H, 3-H), 2.10 (dd, $J = 13$ Hz/6 Hz, 3-H), 3.83 (s, 3H, OCH₃), 4.90 (dd, $J = 16$ Hz/9 Hz, 1H, 4-H), 6.63 (d, $J = 8.8$ Hz, 1H, 8-H), 6.88 (pd, $J = 7.4$ Hz/1.6 Hz, 2H, 4'-H/5'-H), 6.98 (dd, $J = 7.7$ Hz/1.6 Hz, 1H, 3'-H), 7.19 (bs, 1H, CHNHCONHAr), 7.20 (d, $J = 8.5$ Hz, 1H, 7-H), 7.40 (s, 1H, 5-H), 8.01 (s, 1H, CHNHCONHAr), 8.18 (dd, $J = 7.5$ Hz/1.9 Hz, 1H, 6'-H), 9.10 (s, 1H, NHCOOC(CH₃)₃). ¹³C NMR (DMSO-*d*₆) δ 24.6 (CH₃), 28.1 (C(CH₃)₃), 28.9 (CH₃), 40.0 (C-3), 42.2 (C-4), 55.6 (OCH₃), 74.7 (C-2), 78.5 (C(CH₃)₃), 110.5 (C-3'), 116.6 (C-8), 117.8 (C-5/C-6'), 119.6 (C-7), 120.5 (C-5'), 121.0 (C-4'), 122.9 (C-4a), 129.4 (C-1'), 132.0 (C-6), 147.2 (C-2'), 148.6 (C-8a), 153.0 (NHCOOC(CH₃)₃), 155.0 (CHNHCONHAr). Anal. (C₂₄H₃₁N₃O₅) theoretical: C, 65.29; H, 7.08; N, 9.52. Found: C, 65.20; H, 7.09; N, 9.51.

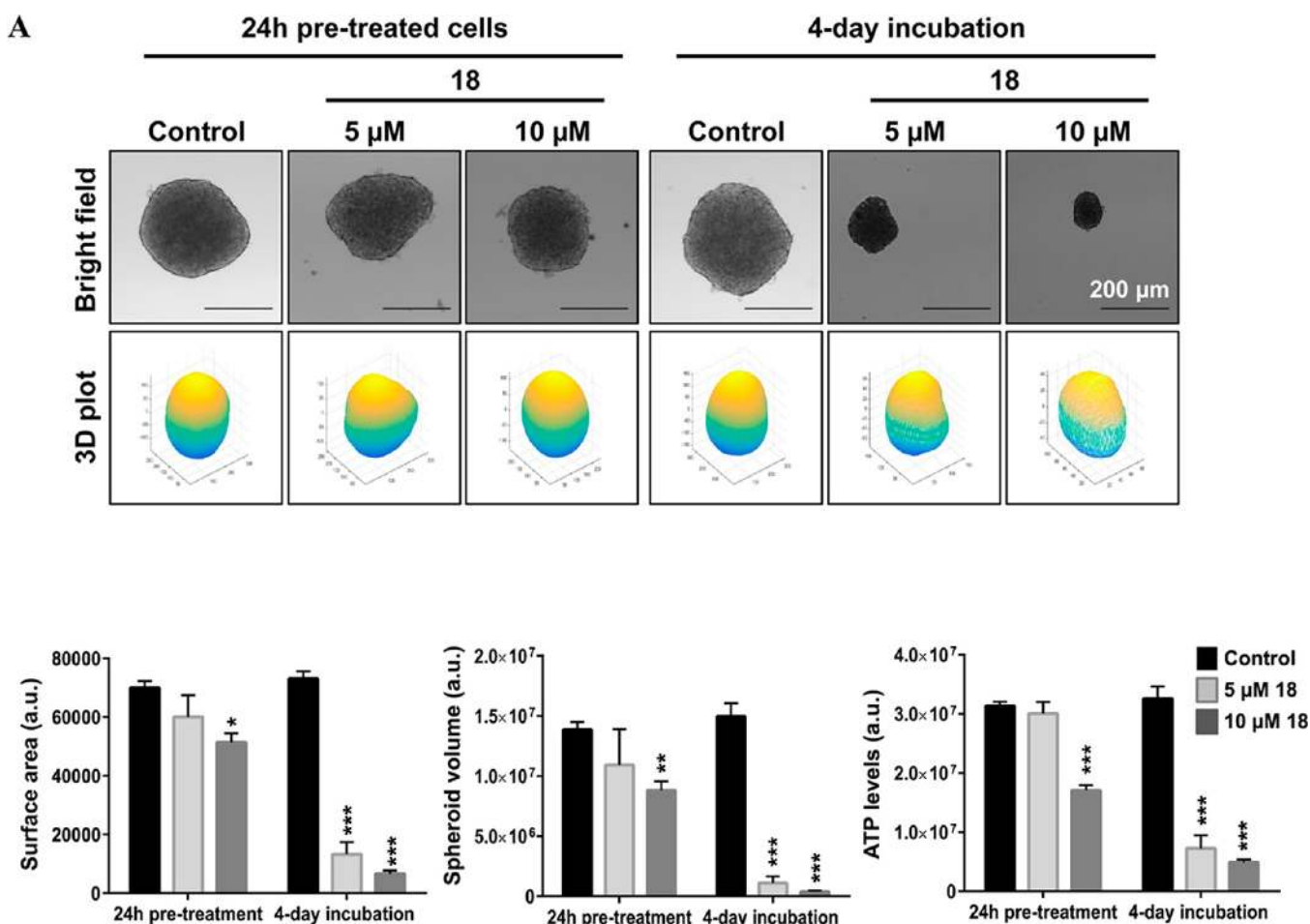


Figure 10. continued

R/S-N-3-Fluorophenyl-N'-(6-tert-butoxycarbonylamino-3,4-dihydro-2,2-dimethyl-2H-1-benzopyran-4-yl)urea (15). The title compound was obtained as described for **10**, starting from **9** (0.2 g, 0.68 mmol) and 3-fluorophenyl isocyanate (0.11 g, 0.82 mmol): mp 115–125 °C; ^1H NMR (DMSO- d_6) δ 1.24 (s, 3H, CH₃), 1.35 (s, 3H, CH₃), 1.42 (s, 9H, NHCOOC(CH₃)₃), 1.70 (dd, J = 13 Hz/11 Hz, 1H, 3-H), 2.08 (dd, J = 13 Hz/6 Hz, 3-H), 4.92 (dd, J = 16 Hz/10 Hz, 1H, 4-H), 6.55 (d, J = 8.6 Hz, 1H, CHNHCONHAr), 6.64 (d, J = 8.7 Hz, 1H, 8-H), 6.73 (t, J = 7.6 Hz, 1H, 4'-H), 7.06 (d, J = 7.8 Hz, 1H, 6'-H), 7.17 (d, J = 7.1 Hz, 1H, 7-H), 7.26 (dd, J = 15.2 Hz/7.7 Hz, 1H, 5'-H), 7.41 (s, 1H, 5-H), 7.53 (d, J = 12 Hz, 1H, 2'-H), 8.73 (s, 1H, CHNHCONHAr), 9.11 (s, 1H, NHCOOC(CH₃)₃). ^{13}C NMR (DMSO- d_6) δ 24.4 (CH₃), 28.1 (C(CH₃)₃), 29.0 (CH₃), 40.0 (C-3), 42.3 (C-4), 74.8 (C-2), 78.5 (C(CH₃)₃), 104.4 (d, J = 27 Hz, C-2'), 107.4 (d, J = 21 Hz, C-4'), 113.5 (d, J = 2 Hz, C-6'), 116.7 (C-8), 117.6 (C-5), 119.6 (C-7), 122.9 (C-4a), 130.1 (d, J = 10 Hz, C-5'), 132.0 (C-6), 142.2 (d, J = 12 Hz, C-1'), 148.5 (C-8a), 152.9 (NHCOOC(CH₃)₃), 154.9 (CHNHCONHAr), 161.5–163.4 (d, J = 240 Hz, C-3'). Anal. (C₂₃H₂₈FN₃O₄) theoretical: C, 64.32; H, 6.57; N, 9.78. Found: C, 64.68; H, 6.26; N, 10.09.

R/S-N-3-Bromophenyl-N'-(6-tert-butoxycarbonylamino-3,4-dihydro-2,2-dimethyl-2H-1-benzopyran-4-yl)urea (17). The title compound was obtained as described for **10**, starting from **9** (0.2 g, 0.68 mmol) and 3-bromophenyl isocyanate (0.16 g, 0.82 mmol): mp 209.5–210.5 °C; ^1H NMR (DMSO- d_6) δ 1.24 (s, 3H, CH₃), 1.35 (s, 3H, CH₃), 1.42 (s, 9H, NHCOOC(CH₃)₃), 1.71 (dd, J = 13 Hz/11 Hz, 1H, 3-H), 2.08 (dd, J = 13 Hz/6 Hz, 3-H), 4.92 (dd, J = 16 Hz/10 Hz, 1H, 4-H), 6.57 (d, J = 8.6 Hz, 1H, CHNHCONHAr), 6.63 (d, J = 8.7 Hz, 1H, 8-H), 7.09 (d, J = 8.5 Hz, 1H, 4'-H), 7.16 (d, J = 7.1 Hz, 1H, 7-H), 7.20 (t, J = 8 Hz, 1H, 5'-H), 7.26 (d, J = 8.7 Hz, 1H, 6'-H), 7.40 (s, 1H, 5-H), 7.90 (t, J = 1.9 Hz, 1H, 2'-H), 8.71 (s, 1H, CHNHCONHAr), 9.09 (s, 1H, NHCOOC(CH₃)₃). ^{13}C NMR (DMSO- d_6) δ 24.4 (CH₃), 28.1

(C(CH₃)₃), 29.0 (CH₃), 40.0 (C-3), 42.4 (C-4), 74.8 (C-2), 78.5 (C(CH₃)₃), 116.6 (C-8/C-6'), 117.5 (C-5), 119.6 (C-7), 120.1 (C-2'), 121.7 (C-3'), 122.9 (C-4a), 123.7 (C-4'), 130.6 (C-5'), 132.0 (C-6), 142.0 (C-1'), 148.5 (C-8a), 152.9 (NHCOOC(CH₃)₃), 154.9 (CHNHCONHAr). Anal. (C₂₃H₂₈BrN₃O₄) theoretical: C, 56.33; H, 5.76; N, 8.57. Found: C, 56.40; H, 5.83; N, 8.44.

R/S-N-3-Nitrophenyl-N'-(6-tert-butoxycarbonylamino-3,4-dihydro-2,2-dimethyl-2H-1-benzopyran-4-yl)urea (19). The title compound was obtained as described for **10**, starting from **9** (0.2 g, 0.68 mmol) and 3-nitrophenyl isocyanate (0.13 g, 0.82 mmol): mp 120–155 °C; ^1H NMR (DMSO- d_6) δ 1.25 (s, 3H, CH₃), 1.36 (s, 3H, CH₃), 1.41 (s, 9H, NHCOOC(CH₃)₃), 1.76 (dd, J = 13 Hz/11 Hz, 1H, 3-H), 2.09 (dd, J = 13 Hz/6 Hz, 3-H), 4.95 (dd, J = 16 Hz/10 Hz, 1H, 4-H), 6.64 (d, J = 8.8 Hz, 1H, 8-H), 6.71 (d, J = 8.7 Hz, 1H, CHNHCONHAr), 7.17 (bs, 1H, 7-H), 7.41 (s, 1H, 5-H), 7.53 (t, J = 8.2 Hz, 1H, 5'-H), 7.69 (d, J = 7.8 Hz, 1H, 4'-H), 7.78 (d, J = 8.1 Hz, 1H, 6'-H), 8.61 (t, J = 2 Hz, 1H, 2'-H), 9.09 (s, 2H, CHNHCONHAr/NHCOOC(CH₃)₃). ^{13}C NMR (DMSO- d_6) δ 24.4 (CH₃), 28.1 (C(CH₃)₃), 29.1 (CH₃), 40.0 (C-3), 42.5 (C-4), 74.8 (C-2), 78.5 (C(CH₃)₃), 111.7 (C-2'), 115.7 (C-6'), 116.7 (C-8), 117.5 (C-5), 119.6 (C-7), 122.8 (C-4a), 123.9 (C-4'), 129.9 (C-5'), 132.0 (C-6), 141.7 (C-1'), 148.1 (C-3'), 148.5 (C-8a), 152.9 (NHCOOC(CH₃)₃), 154.9 (CHNHCONHAr). Anal. (C₂₃H₂₈N₄O₆) theoretical: C, 60.52; H, 6.18; N, 12.27. Found: C, 61.01; H, 6.13; N, 12.18.

R/S-N-3-Trifluoromethylphenyl-N'-(6-tert-butoxycarbonylamino-3,4-dihydro-2,2-dimethyl-2H-1-benzopyran-4-yl)urea (20). The title compound was obtained as described for **10**, starting from **9** (0.2 g, 0.68 mmol) and 3-trifluoromethylphenyl isocyanate (0.15 g, 0.82 mmol): mp 140–155 °C; ^1H NMR (DMSO- d_6) δ 1.25 (s, 3H, CH₃), 1.36 (s, 3H, CH₃), 1.42 (s, 9H, NHCOOC(CH₃)₃), 1.74 (dd, J = 13 Hz/11 Hz, 1H, 3-H), 2.09 (dd, J = 13 Hz/6 Hz, 3-H), 4.94 (dd,

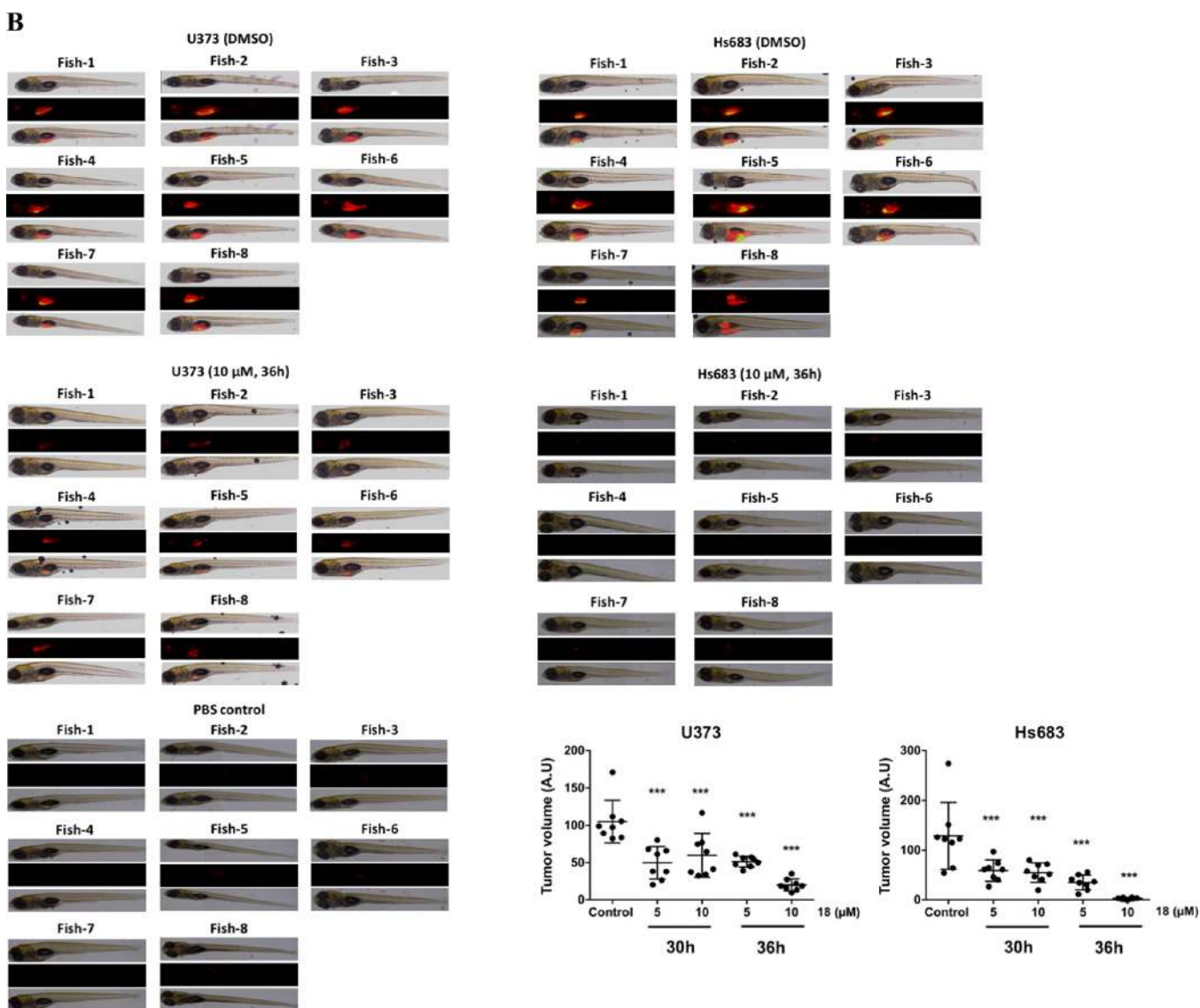


Figure 10. Antitumor potential of compound 18. (A) Representative bright field images and 3D plots of spheroids generated from Hs683 cells (top panels). Cells were pretreated for 24 h with the indicated concentrations of 18 and then left untreated for 96 h (4-day incubation, upper left panel), or untreated cells were cultured for 96 h in the presence of the indicated concentrations of 18 (24 h pretreated cells, upper right panel). The surface, volume, and ATP levels of spheroids were measured as described in the [Experimental Section](#) (bottom panels). Data are the mean \pm SD of three independent experiments. (B) Fluorescent Hs683 and U373 cells were treated, or not, in vitro at 5 or 10 μ M compound 18 for 30 or 36 h and then injected in the zebrafish yolk sac. The figure represents results obtained with a pretreatment of 36 h at 10 μ M; for the other conditions of treatment we refer to [Figure SI-5](#). After 72 h, fluorescence was quantified and representative images from a total of eight fish per condition are shown. For each fish, the upper panel represents the bright field, the middle panel the red fluorescence, and the bottom panel the merged picture. Fluorescence intensity quantification graphs are shown. PBS injection was used as a control for injection side effects. *, **, *** indicate $p < 0.05$, $p < 0.01$, $p < 0.001$ compared to control cells, respectively.

$J = 16$ Hz/10 Hz, 1H, 4-H), 6.62 (d, $J = 8.6$ Hz, 1H, CHNHCONHAr), 6.64 (d, $J = 8.8$ Hz, 1H, 8-H), 7.17 (bd, $J = 6.7$ Hz, 1H, 7-H), 7.26 (d, $J = 7.5$ Hz, 1H, 4'-H), 7.41 (s, 1H, 5-H), 7.47 (t, $J = 7.9$ Hz, 1H, 5'-H), 7.53 (d, $J = 8.2$ Hz, 1H, 6'-H), 8.07 (s, 1H, 2'-H), 8.89 (s, 1H, CHNHCONHAr), 9.08 (s, 1H, NHCOOC(CH₃)₃). ¹³C NMR (DMSO-*d*₆) δ 24.4 (CH₃), 28.1 (C(CH₃)₃), 29.1 (CH₃), 40.0 (C-3), 42.4 (C-4), 74.8 (C-2), 78.5 (C(CH₃)₃), 113.8 (C-2'), 116.6 (C-8), 117.4 (C-5/C-4'), 119.6 (C-7), 121.3 (C-6'), 122.9 (C-4a), 123.2–125.4 (d, $J = 272$ Hz, CF₃), 129.3–129.6 (d, $J = 31$ Hz, C-3'), 129.7 (C-5'), 132.0 (C-6), 141.2 (C-1'), 148.5 (C-8a), 153.0 (NHCOOC(CH₃)₃), 155.0 (CHNHCONHAr). Anal. (C₂₄H₂₈F₃N₃O₄) theoretical: C, 60.12; H, 5.89; N, 8.76. Found: C, 60.19; H, 6.03; N, 8.59.

R/S-N-3-Methoxyphenyl-N'-(6-tert-butoxycarbonylamino-3,4-dihydro-2,2-dimethyl-2H-1-benzopyran-4-yl)urea (21). The title compound was obtained as described for 10, starting from 9 (0.2 g,

0.68 mmol) and 3-methoxyphenyl isocyanate (0.12 g, 0.82 mmol): mp 189–191 °C; ¹H NMR (DMSO-*d*₆) δ 1.24 (s, 3H, CH₃), 1.35 (s, 3H, CH₃), 1.42 (s, 9H, NHCOOC(CH₃)₃), 1.68 (dd, $J = 13$ Hz/11 Hz, 1H, 3-H), 2.08 (dd, $J = 13$ Hz/6 Hz, 3-H), 3.72 (s, 1H, OCH₃), 4.91 (dd, $J = 16$ Hz/10 Hz, 1H, 4-H), 6.46 (d, $J = 8.7$ Hz, 1H, CHNHCONHAr), 6.50 (dd, $J = 8.2$ Hz/1.9 Hz, 1H, 4'-H), 6.63 (d, $J = 8.8$ Hz, 1H, 8-H), 6.89 (dd, $J = 8.1$ Hz/1 Hz, 1H, 6'-H), 7.13 (t, $J = 8$ Hz, 1H, 5'-H), 7.17 (d, $J = 7.8$ Hz, 1H, 7-H), 7.22 (t, $J = 2$ Hz, 1H, 2'-H), 7.40 (s, 1H, 5-H), 8.52 (s, 1H, CHNHCONHAr), 9.08 (s, 1H, NHCOOC(CH₃)₃). ¹³C NMR (DMSO-*d*₆) δ 24.5 (CH₃), 28.1 (C(CH₃)₃), 29.0 (CH₃), 40.0 (C-3), 42.3 (C-4), 54.8 (OCH₃), 74.8 (C-2), 78.5 (C(CH₃)₃), 103.4 (C-2'), 106.7 (C-4'), 110.1 (C-6'), 116.6 (C-8), 117.6 (C-5), 119.6 (C-7), 123.0 (C-4a), 129.4 (C-5'), 132.0 (C-6), 141.6 (C-1'), 148.6 (C-8a), 153.0 (NHCOOC(CH₃)₃), 155.0 (CHNHCONHAr), 159.7 (C-3').

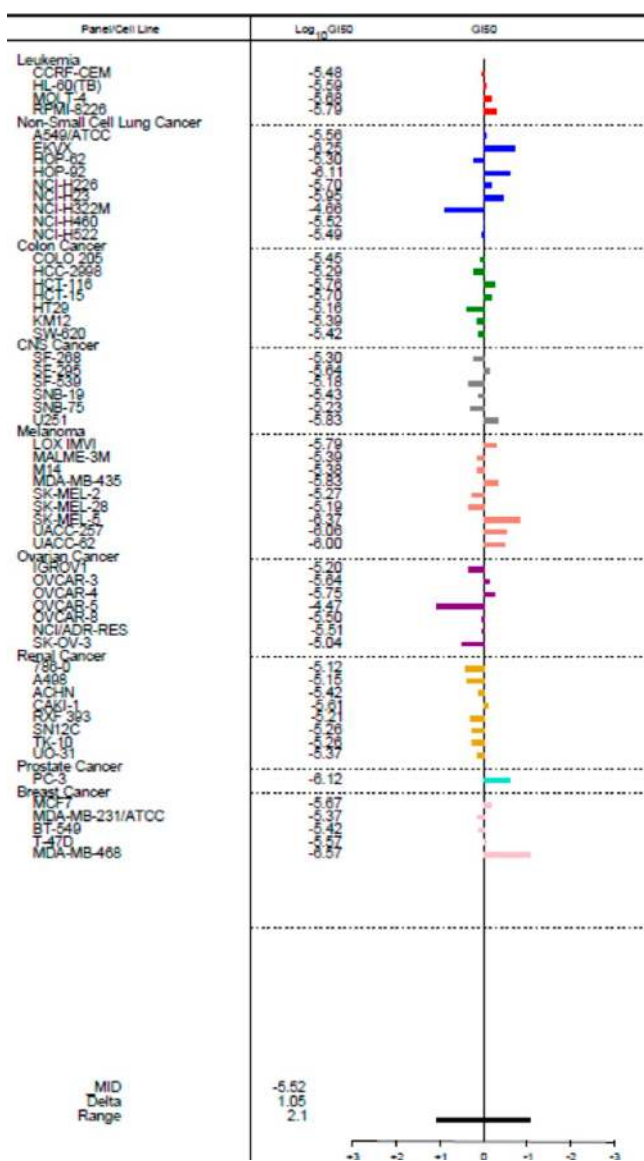


Figure 11. Characterization of the growth inhibitory effects exerted by compound **18** in the NCI 60-cell-line panel (National Cancer Institute Developmental Therapeutics Program, mean graphs).

Anal. ($C_{24}H_{31}N_3O_5$) theoretical: C, 65.29; H, 7.08; N, 9.52. Found: C, 65.25; H, 7.13; N, 9.43.

R/S-N-3-Aminomethylphenyl-N'-(6-tert-butoxycarbonylamino-3,4-dihydro-2,2-dimethyl-2H-1-benzopyran-4-yl)urea (22). Raney nickel was added to a solution of **18** (0.3 g, 0.69 mmol) and ammonia (0.3 mL) in ethanol (10 mL). The solution was stirred in a sealed hydrogenator under a hydrogen pressure of 7 bar. When the reaction was ended (3 h), the catalyst was filtered off and the filtrate was evaporated under pressure. The title compound was obtained after purification on a DCVC system: mp 120–170 °C; 1H NMR (DMSO- d_6) δ 1.24 (s, 3H, CH_3), 1.35 (s, 3H, CH_3), 1.42 (s, 9H, $NHCOOC(CH_3)_3$), 1.68 (dd, $J = 13$ Hz/11 Hz, 1H, 3- H), 2.09 (dd, $J = 13$ Hz/6 Hz, 3- H), 3.3 (bs, 2H, CH_2NH_2), 3.67 (s, 2H, CH_2NH_2), 4.91 (dd, $J = 16$ Hz/10 Hz, 1H, 4- H), 6.47 (d, $J = 8.7$ Hz, 1H, $CHNHCONHAr$), 6.63 (d, $J = 8.8$ Hz, 1H, 8- H), 6.89 (d, $J = 7.5$ Hz, 1H, 4'- H), 7.17 (m, 2H, 7- H /5'- H), 7.31 (d, $J = 8.2$ Hz, 1H, 6'- H), 7.37 (s, 1H, 2'- H), 7.41 (s, 1H, 5- H), 8.46 (s, 1H, $CHNHCONHAr$), 9.08 (s, 1H, $NHCOOC(CH_3)_3$). ^{13}C NMR (DMSO- d_6) δ 24.5 (CH_3), 28.1 ($C(CH_3)_3$), 29.0 (CH_3), 40.0 (C-3), 42.3 (C-4), 45.7 (CH_2NH_2), 74.8 (C-2), 78.5 ($C(CH_3)_3$), 115.8 (C-6'), 116.5 (C-2'), 116.7 (C-8), 117.5 (C-5), 119.6 (C-7), 120.0 (C-4'), 123.0 (C-4a), 128.4 (C-5'), 132.0 (C-6), 140.2 (C-1'), 144.5 (C-3'), 148.6 (C-8a), 153.0

($NHCOOC(CH_3)_3$), 155.1 ($CHNHCONHAr$). Anal. ($C_{24}H_{32}N_4O_4$) theoretical: C, 65.43; H, 7.32; N, 12.72. Found: C, 64.96; H, 7.31; N, 12.70.

R/S-N-3-Aminophenyl-N'-(6-tert-butoxycarbonylamino-3,4-dihydro-2,2-dimethyl-2H-1-benzopyran-4-yl)urea (23). Ammonium chloride (0.15 g, 2.83 mmol) and iron (0.6 g, 10.7 mmol) were added to a solution of **19** (0.3 g, 0.66 mmol) in ethanol/water 3:1 (10 mL). The solution was heated at 80 °C for 15 min. After filtration (without cooling), the filtrate was treated with charcoal, filtered, and evaporated under vacuum. The title compound was obtained after purification on a DCVC system: mp 130–140 °C; 1H NMR (DMSO- d_6) δ 1.24 (s, 3H, CH_3), 1.35 (s, 3H, CH_3), 1.43 (s, 9H, $NHCOOC(CH_3)_3$), 1.65 (dd, $J = 13$ Hz/11 Hz, 1H, 3- H), 2.08 (dd, $J = 13$ Hz/6 Hz, 3- H), 4.89 (dd, $J = 16$ Hz/10 Hz, 1H, 4- H), 4.95 (s, 1H, NH_2), 6.14 (dd, $J = 7.9$ Hz/1.3 Hz, 1H, 4'- H), 6.35 (d, $J = 8.7$ Hz, 1H, $CHNHCONHAr$), 6.57 (dd, $J = 8.1$ Hz/1 Hz, 1H, 6'- H), 6.63 (d, $J = 8.8$ Hz, 1H, 8- H), 6.72 (t, $J = 1.9$ Hz, 1H, 2'- H), 6.85 (t, $J = 8$ Hz, 1H, 5'- H), 7.17 (d, $J = 6.6$ Hz, 1H, 7- H), 7.39 (s, 1H, 5- H), 8.17 (s, 1H, $CHNHCONHAr$), 9.10 (s, 1H, $NHCOOC(CH_3)_3$). ^{13}C NMR (DMSO- d_6) δ 24.6 (CH_3), 28.1 ($C(CH_3)_3$), 29.0 (CH_3), 40.0 (C-3), 42.2 (C-4), 74.8 (C-2), 78.5 ($C(CH_3)_3$), 103.4 (C-2'), 105.8 (C-6'), 107.6 (C-4'), 116.6 (C-8), 117.7 (C-5), 119.6 (C-7), 123.1 (C-4a), 128.9 (C-5'), 132.0 (C-6), 140.9 (C-1'), 148.6 (C-8a), 149.0 (C-3'), 153.0 ($NHCOOC(CH_3)_3$), 154.9 ($CHNHCONHAr$). Anal. ($C_{23}H_{30}N_4O_4$) theoretical: C, 64.77; H, 7.09; N, 13.14. Found: C, 64.32; H, 7.06; N, 12.95.

R/S-N-4-Nitrophenyl-N'-(6-tert-butoxycarbonylamino-3,4-dihydro-2,2-dimethyl-2H-1-benzopyran-4-yl)urea (26). The title compound was obtained as described for **10**, starting from **9** (0.2 g, 0.68 mmol) and 4-nitrophenyl isocyanate (0.13 g, 0.82 mmol): mp 233–233.5 °C; 1H NMR (DMSO- d_6) δ 1.25 (s, 3H, CH_3), 1.36 (s, 3H, CH_3), 1.42 (s, 9H, $NHCOOC(CH_3)_3$), 1.75 (dd, $J = 13$ Hz/11 Hz, 1H, 3- H), 2.10 (dd, $J = 13$ Hz/6 Hz, 3- H), 4.94 (dd, $J = 16$ Hz/9 Hz, 1H, 4- H), 6.64 (d, $J = 8.8$ Hz, 1H, 8- H), 6.82 (d, $J = 8.6$ Hz, 1H, $CHNHCONHAr$), 7.18 (d, $J = 6.5$ Hz, 1H, 7- H), 7.40 (s, 1H, 5- H), 7.69 (d, $J = 7.7$ Hz, 2H, 2'- H /6'- H), 8.17 (d, $J = 9.3$ Hz, 2H, 3'- H /5'- H), 9.09 (s, 1H, $NHCOOC(CH_3)_3$), 9.32 (s, 1H, $CHNHCONHAr$). ^{13}C NMR (DMSO- d_6) δ 24.4 (CH_3), 28.1 ($C(CH_3)_3$), 29.0 (CH_3), 40.4 (C-3), 42.5 (C-4), 74.8 (C-2), 78.6 ($C(CH_3)_3$), 116.7 (C-8), 117.0 (C-2'/C-6'), 117.5 (C-5), 119.6 (C-7), 122.5 (C-4a), 125.1 (C-3'/C-5'), 132.1 (C-6), 140.5 (C-1'), 147.0 (C-4'), 148.5 (C-8a), 152.9 ($NHCOOC(CH_3)_3$), 154.4 ($CHNHCONHAr$). Anal. ($C_{23}H_{28}N_4O_6$) theoretical: C, 60.52; H, 6.18; N, 12.27. Found: C, 59.95; H, 6.16; N, 12.09.

R/S-N-4-Trifluoromethylphenyl-N'-(6-tert-butoxycarbonylamino-3,4-dihydro-2,2-dimethyl-2H-1-benzopyran-4-yl)urea (27). The title compound was obtained as described for **10**, starting from **9** (0.2 g, 0.68 mmol) and 4-trifluoromethylphenyl isocyanate (0.15 g, 0.82 mmol): mp 186–188 °C; 1H NMR (DMSO- d_6) δ 1.25 (s, 3H, CH_3), 1.36 (s, 3H, CH_3), 1.42 (s, 9H, $NHCOOC(CH_3)_3$), 1.72 (dd, $J = 13$ Hz/11 Hz, 1H, 3- H), 2.09 (dd, $J = 13$ Hz/6 Hz, 3- H), 4.94 (dd, $J = 16$ Hz/9 Hz, 1H, 4- H), 6.63–6.66 (m, 2H, $CHNHCONHAr$ /8- H), 7.18 (d, $J = 7$ Hz, 1H, 7- H), 7.40 (s, 1H, 5- H), 7.59 (d, $J = 8.8$ Hz, 2H, 3'- H /5'- H), 7.65 (d, $J = 8.8$ Hz, 1H, 2'- H /6'- H), 8.95 (s, 1H, $CHNHCONHAr$), 9.09 (s, 1H, $NHCOOC(CH_3)_3$). ^{13}C NMR (DMSO- d_6) δ 24.4 (CH_3), 28.1 ($C(CH_3)_3$), 29.0 (CH_3), 40.4 (C-3), 42.4 (C-4), 74.8 (C-2), 78.5 ($C(CH_3)_3$), 116.7 (C-8), 117.4 (C-5/C-2'/C-6'), 119.6 (C-7), 121.0–121.2 (d, $J = 32$ Hz, C-4'), 122.8 (C-4a), 123.5–125.7 (d, $J = 271$ Hz, CF_3), 126.0 (C-3'/C-5'), 132.0 (C-6), 144.1 (C-1'), 148.6 (C-8a), 153.0 ($NHCOOC(CH_3)_3$), 154.8 ($CHNHCONHAr$). Anal. ($C_{24}H_{28}F_3N_4O_6$) theoretical: C, 60.12; H, 5.89; N, 8.76. Found: C, 60.08; H, 5.97; N, 8.72.

R/S-N-4-Methoxyphenyl-N'-(6-tert-butoxycarbonylamino-3,4-dihydro-2,2-dimethyl-2H-1-benzopyran-4-yl)urea (28). The title compound was obtained as described for **10**, starting from **9** (0.2 g, 0.68 mmol) and 4-methoxyphenyl isocyanate (0.12 g, 0.82 mmol): mp 204–205 °C; 1H NMR (DMSO- d_6) δ 1.24 (s, 3H, CH_3), 1.35 (s, 3H, CH_3), 1.43 (s, 9H, $NHCOOC(CH_3)_3$), 1.68 (dd, $J = 13$ Hz/11 Hz, 1H, 3- H), 2.06 (dd, $J = 13$ Hz/6 Hz, 3- H), 3.70 (s, 3H, OCH_3), 4.91 (dd, $J = 16$ Hz/9 Hz, 1H, 4- H), 6.47 (d, $J = 8.7$ Hz, 1H, $CHNHCONHAr$), 6.62 (d, $J = 8.8$ Hz, 1H, 8- H), 6.83 (d, $J = 9$ Hz, 2H, 3'- H /5'- H), 7.16 (d, $J = 7.2$ Hz, 7- H), 7.35 (d, $J = 9$ Hz, 2H, 2'- H /6'- H), 7.40 (s, 1H, 5- H), 8.41

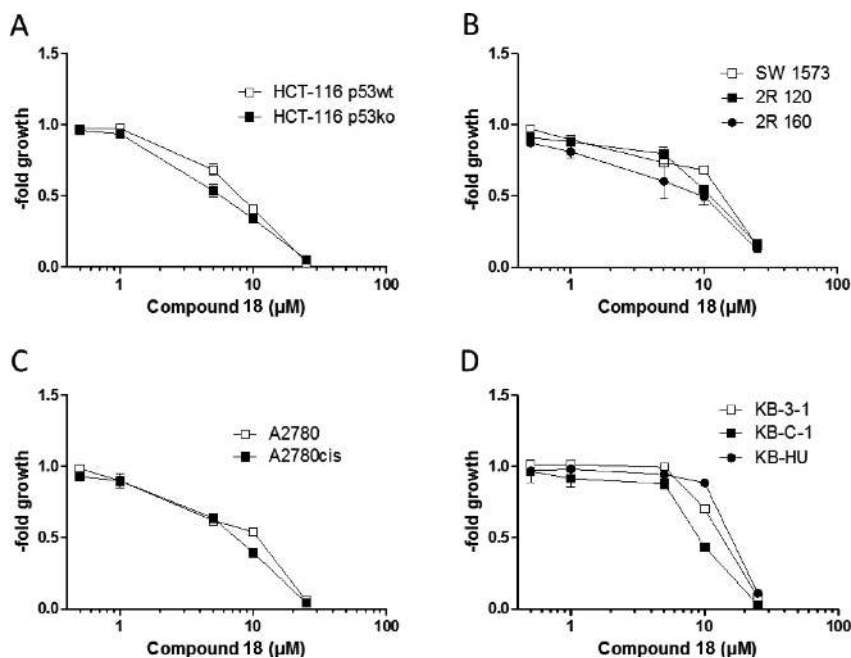


Figure 12. Impact of clinically significant drug resistance mechanisms on the anticancer activity of 18. (A) HCT-116 p53wt and HCT-116 p53ko (p53 knockout), (B) SW1573, SW1573 2R120 (ABCC1- and LRP-overexpressing) and 2R160 (ABCB1-overexpressing), (C) A2780 and A2780cis (cisplatin resistant), and (D) KB-3-1, KB-C-1 (ABCB1-overexpressing) and KB-HU (ribonucleotide reductase subunit 2-overexpressing) were treated with the indicated concentrations of compound 18. After 72 h of continuous drug exposure, cell viability was determined by MTT assay. The experiments were performed in quintuplicate, and results are shown as the mean \pm SD.

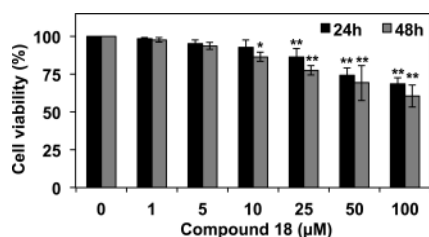


Figure 13. Effect of compound 18 on the viability of healthy peripheral blood mononuclear cells. Histograms correspond to the mean \pm SD of three independent experiments. *, ** indicate $p < 0.05$, $p < 0.01$ compared to control cells, respectively.

(s, 1H, CHNHCONHAr), 9.08 (s, 1H, NHCOOC(CH₃)₃). ¹³C NMR (DMSO-*d*₆) δ 24.4 (CH₃), 28.1 (C(CH₃)₃), 29.1 (CH₃), 40.0 (C-3), 42.3 (C-4), 55.1 (OCH₃), 74.8 (C-2), 78.5 (C(CH₃)₃), 113.8 (C-3'/C-5'), 116.6 (C-8), 117.7 (C-5), 119.5 (C-2'/C-6'), 119.6 (C-7), 123.3 (C-4a), 132.0 (C-6), 133.6 (C-1'), 148.6 (C-8a), 153.0 (NHCOOC(CH₃)₃), 154.0 (CHNHCONHAr), 155.4 (C-4'). Anal. (C₂₄H₃₁N₃O₅) theoretical: C, 65.29; H, 7.08; N, 9.52. Found: C, 64.88; H, 7.20; N, 9.13.

R/S-N-3-Cyanophenyl-N'-(3,4-dihydro-2,2-dimethyl-2H-1-benzopyran-4-yl)urea (32). The title compound was obtained as described for 10, starting from 31 (0.2 g, 1.13 mmol) and 3-cyanophenyl isocyanate (0.18 g, 1.25 mmol): mp 217–219 °C; ¹H NMR (DMSO-*d*₆) δ 1.28 (s, 3H, CH₃), 1.39 (s, 3H, CH₃), 1.77 (t, *J* = 12 Hz, 1H, 3-H), 2.12 (dd, *J* = 13 Hz/6.2 Hz, 3-H), 4.98 (dd, *J* = 16.3 Hz/9.2 Hz, 1H, 4-H), 6.74 (d, *J* = 8.7 Hz, 1H, 8-H), 6.76 (d, *J* = 10 Hz, 1H, CHNHCONHAr), 6.88 (t, *J* = 7.4 Hz, 1H, 6-H), 7.14 (t, *J* = 7.6 Hz, 1H, 7-H), 7.26 (d, *J* = 7.6 Hz, 1H, 5-H), 7.37 (d, *J* = 7.5 Hz, 1H, 4'-H), 7.46 (t, *J* = 8 Hz, 1H, 5'-H), 7.64 (d, *J* = 8.3 Hz, 1H, 6'-H), 8.00 (s, 1H, 2'-H), 8.92 (s, 1H, CHNHCONHAr). ¹³C NMR (DMSO-*d*₆) δ 25.0 (CH₃), 29.6 (CH₃), 40.0 (C-3), 42.8 (C-4), 75.6 (C-2), 117.2 (C-8), 119.4 (CN), 120.4 (C-6), 120.8 (C-2'), 122.9 (C-6'), 123.7 (C-4a), 125.1 (C-4'), 128.0 (C-5), 129.0 (C-7), 130.6 (C-5'), 141.8 (C-1'), 153.8 (C-8a), 155.5 (CHNHCONHAr). Anal. (C₁₉H₁₉N₃O₂) theoretical: C, 71.01; H, 5.96; N, 13.08. Found: C, 70.90; H, 5.97; N, 12.83.

R/S-N-3-Cyanophenyl-N'-(6-amino-3,4-dihydro-2,2-dimethyl-2H-1-benzopyran-4-yl)urea (33). A suspension of 18 (2.85 g, 6.5 mmol) in a 5 N hydrochloric acid ethanolic solution (100 mL) was heated for 5 min. The mixture was then poured into water (200 mL). The title compound was precipitated by addition of a 20% aqueous solution of sodium hydroxide until pH = 10, filtered, washed with water, and dried: mp 176–178 °C; ¹H NMR (DMSO-*d*₆) δ 1.21 (s, 3H, CH₃), 1.32 (s, 3H, CH₃), 1.67 (dd, *J* = 13 Hz/11 Hz, 1H, 3-H), 2.03 (dd, *J* = 13 Hz/6.3 Hz, 3-H), 4.57 (s, 2H, NH₂), 4.87 (dd, *J* = 15.9 Hz/9.7 Hz, 1H, 4-H), 6.40 (dd, *J* = 8.5 Hz/2.5 Hz, 1H, 7-H), 6.45 (d, *J* = 8.5 Hz, 1H, 8-H), 6.51 (d, *J* = 2.2 Hz, 1H, 5-H), 6.63 (d, *J* = 8.7 Hz, 1H, CHNHCONHAr), 7.36 (d, *J* = 7.7 Hz, 1H, 4'-H), 7.45 (t, *J* = 8 Hz, 1H, 5'-H), 7.63 (d, *J* = 8.3 Hz, 1H, 6'-H), 8.00 (s, 1H, 2'-H), 8.86 (s, 1H, CHNHCONHAr). ¹³C NMR (DMSO-*d*₆) δ 24.8 (CH₃), 29.6 (CH₃), 40.8 (C-3), 42.9 (C-4), 74.4 (C-2), 112.0 (C-3'), 112.7 (C-5), 115.7 (C-7), 117.4 (C-8), 119.5 (CN), 120.7 (C-2'), 122.8 (C-6'), 123.4 (C-4a), 125.1 (C-4'), 130.6 (C-5'), 141.8 (C-6), 142.2 (C-1'), 144.8 (C-8a), 155.4 (CHNHCONHAr). Anal. (C₁₉H₂₀N₄O₂) theoretical: C, 67.84; H, 5.99; N, 16.66. Found: C, 67.47; H, 6.03; N, 16.53.

R/S-N-3-Cyanophenyl-N'-(6-formamido-3,4-dihydro-2,2-dimethyl-2H-1-benzopyran-4-yl)urea (34). A mixture of acetic anhydride (2 mL, 21.2 mmol) and formic acid (1 mL, 26.5 mmol) was heated at 55 °C for 2 h. The mixture was then cooled to 0 °C, and anhydrous THF (2 mL) was added. A solution of 33 (0.3 g, 0.89 mmol) in anhydrous THF was added dropwise. When the reaction was complete, water was added and the resulting precipitate was filtered, washed with water, and dried. The title product was obtained from the crude product by DCVC purification: mp 200–202 °C; ¹H NMR (DMSO-*d*₆) δ 1.26 (s, 3H, CH₃), 1.37 (s, 3H, CH₃), 1.76 (t, *J* = 12 Hz, 1H, 3-H), 2.09 (dd, *J* = 13 Hz/6.2 Hz, 3-H), 4.96 (dd, *J* = 15.3 Hz/10.3 Hz, 1H, 4-H), 6.70 (d, *J* = 8.7 Hz, 1H, 8-H), 6.80 (d, *J* = 8.7 Hz, 1H, CHNHCONHAr), 7.37 (d, *J* = 7.7 Hz, 1H, 4'-H), 7.42–7.48 (m, 3H, 5-H/7-H/5'-H), 7.66 (m, 1H, 6'-H), 8.01 (s, 1H, 2'-H), 8.15 (d, *J* = 2 Hz, 1H, NHCHO), 8.96 (s, 1H, CHNHCONHAr), 10.00 (s, 1H, NHCHO). ¹³C NMR (DMSO-*d*₆) δ 24.4 (CH₃), 29.1 (CH₃), 40.0 (C-3), 42.3 (C-4), 75.1 (C-2), 111.5 (C-3'), 116.8 (C-8), 118.3 (C-5), 119.0 (CN), 120.2 (C-7), 120.3 (C-2'), 122.4 (C-6'), 123.2 (C-4a), 124.0 (C-4'), 124.7 (C-4'), 130.1 (C-5'), 131.0 (C-6), 141.2 (C-1'), 149.5

(C-8a), 154.9 (CHNHCONHAr), 158.9 (NHCHO). Anal. (C₁₉H₂₀N₄O₅) theoretical: C, 65.92; H, 5.53; N, 15.38. Found: C, 65.43; H, 5.55; N, 15.37.

Docking Studies. AutoDock Vina software (The Scripps Research Institute, CA, USA)⁴⁹ was used in the docking studies. Initial structures of SIRT1 and SIRT2 were obtained from the Protein Data Bank (PDB), and coordinates for the compounds were generated using the GlycoBioChem PRODRG2 server.³⁶ To prepare the structure for docking, the ligand and all water molecules were removed. The size of the docking grid was 40 Å × 40 Å × 40 Å, which encompassed most of the entire structures of SIRT1 and -2. AutoDock Vina program was run with four-way multithreading, and the other parameters were default settings in AutoDock Vina program. Figures were generated using PyMol (DeLano, W. L. *The PyMol Molecular Graphics System*; DeLano Scientific: Palo Alto, CA, USA, 2002) and LigPlot+.³⁷

Pharmacology. Cell Cultures and Media. Three human glioma cell lines were used (the Hs683 oligodendroglial and the U373 and T98G glioblastoma models). The biological and histopathological characteristics demonstrating the oligodendroglial nature of the Hs683 model were provided by Le Mercier et al.³⁸ A controversy exists today about the origin of the U373 cells, which are in fact U251 glioblastoma cells.³⁹ A new U373 cell line has been established and deposited at the European Collection of Cell Cultures (Salisbury, U.K.; code ECACC 08061901). We used this U373 model in the current study. The T98G glioma cell line was obtained from the American Type Culture Collection (Manassas, VA, USA; code ATCC CRL-1690) and was initially described by Stein.⁴⁰ The Hs683 model was also obtained from the ATCC (code HTB-138). The uterine cervix carcinoma-derived cell line KB-3-1 and its ABCB1-overexpressing MDR subline KB-C-1 were provided by Dr. Shen (Bethesda, MD, USA).⁴¹ The KB-3-1 derivative KB-HU selected against hydroxyurea was generously donated by Dr. Y. C. Cheng (Yale University, New Haven, CT, USA).³⁵ The ovarian cancer cell line A2780 and its cisplatin resistant subline A2780/cis were purchased from Sigma (Bornem, Belgium). The human colon cancer cell line HCT116 p53 wild-type and its p53/ko clone with deleted p53 were generously donated by Dr. B. Vogelstein (Johns Hopkins University, Baltimore, MD, USA).⁴² The non-small-cell lung cancer cell model SW1573 with its ABCB1- and LRP-overexpressing subline 2R120 and its ABCB1-overexpressing subline 2R160 is from H. Broxterman (Department of Medical Oncology, Free University Hospital, Amsterdam, The Netherlands).⁴³

PBMCs from healthy donors were isolated as previously reported.⁴⁴ Normal astrocytes from murine origin were established and cultured as previously described.⁴⁵

Cells were grown in RPMI 1640 (BioWhittaker, Lonza, Verviers, Belgium) supplemented with 10% heat-inactivated fetal calf serum (BioWhittaker) and 1% antibiotic-antimycotic (BioWhittaker) at 37 °C in humid atmosphere and 5% CO₂. PBMC viability was evaluated as previously described.⁴⁴

1 (Sigma), 2 (Santa Cruz Biotechnology, Heidelberg, Germany), 3 (Sigma), 4 (Enzo Life Sciences, Antwerpen, Belgium), 38 (Cayman, Bio-connect, Huissen, The Netherlands), and all 2,2-dimethylchromans-related compounds were dissolved in DMSO.

Quantitative Videomicroscopy. For videomicroscopic evaluation of the in vitro anticancer effects of 18, cells were cultured in 25 cm² flasks. Time-lapse acquisition of phase contrast microscopy pictures was automatically recorded every 4 min over a 72 h period in triplicate.^{30,46–48} Quantitative data have been obtained by the counting of the number of cells on the pictures over time as previously described^{30,46,48} and detailed in the legends of the figures.

MTT Colorimetric Assay. The MTT colorimetric assay was performed as previously described after 72 h of exposure to the compounds.^{30,46,48} Briefly, cells were seeded in 96-well plates 24 h before treatments. Concentrations of the compounds tested range from 0.01 to 100 μM for 72 h. The growth inhibitory concentration, i.e., the GI₅₀ is the concentration of a compound that decreased by 50% the optical density in comparison to the untreated control condition. Experiments on Hs683, T98G, and U373 cells were conducted once in sextuplicate.

Cell Cycle Analysis. Cell cycle distribution was analyzed as previously described.³²

SA-β-gal Assay. The assessment of senescence was performed using an SA-β-gal assay described elsewhere.³²

Monitoring Cell Proliferation in SIRT1- or SIRT2-Depleted Cells. Cells in 12-well plates were transfected with small interfering RNAs [siRNAs; Qiagen, Venlo, The Netherlands: SiSIRT1_1 (SI00098434), SiHDAC1_2 (SI00098448), siSIRT2_1 (SI00098406), siSIRT2_2 (SI02655471), control siRNA (AllStars Negative Control siRNA)] as described elsewhere.⁴⁹ Gene silencing effects on glioblastoma cell proliferation were recorded and quantified by time-lapse phase contrast videomicroscopy using InCuCyte live-cell imaging system (Essen Bioscience Inc., Hertfordshire, U.K.).

Generation of U373 and Hs683 Spheroids. Spheroids were generated as previously described elsewhere⁴⁹ using a starting cell suspension of 1 × 10³ cells in 25 μL. The volume of multicellular spheroids expressed in voxels (3D pixels) was determined through the generation of 3D plots using the ReViSP software after an initial segmentation with ImageJ software (U.S. National Institutes of Health, Bethesda, MD, USA) as described elsewhere.⁵⁰

ATP Measurement in 3D Spheroid Culture. ATP levels were measured using the CellTiter-Glo 3D cell viability assay (Promega, Leiden, The Netherlands) according to the manufacturer's instructions. Briefly, spheroids were harvested and then mixed with CellTiter-Glo 3D reagent. After shaking for 5 min and stabilizing for 25 min, luminescence signal was measured with a luminometer (Centro LB 960, Berthold Technologies, Korea).

Zebrafish Assay. Wild type zebrafish (*Danio rerio*) were obtained from the Zebrafish International Resource Center (ZIRC, University of Oregon, OR), maintained according to SNU guidelines at 28.5 °C with 10 h dark/14 h light cycles. Zebrafish experiments were carried out as previously described⁵¹ except that cells were fluorescently labeled with CM-Dil (Invitrogen, Korea) 2 h prior to injection. For CM-Dil labeled cancer cell injection, micropipettes for injection and anesthesia were generated from a 1.0 mm glass capillary (World Precision Instruments, Sarasota, FL, USA) by using a micropipette puller (Shutter Instrument, Novato, CA, USA). 48 h after fertilization, zebrafish were anesthetized in 0.02% tricaine (Sigma) and immobilized on an agar plate. 100–200 of CM-Dil labeled cancer cells are also stained with 0.05% of phenol red solution (Sigma) for better visualization during injection into the yolk sac. After injection, zebrafish were incubated in 24-well plates containing Danieau solution with 0.003% phenylthiourea (Sigma, USA) at 28.5 °C for 72 h. Pictures were taken by fixing zebrafish embryos onto a glass slide with 3% methylcellulose (Sigma).

In Vitro HDAC Activity Assay. Assays were carried out as previously described.^{52,53} IC₅₀ values were determined using the GraphPad Prism 6.0 software.

Western Blot Analysis. For the preparation of total proteins, cells were harvested, washed in cold 1× PBS, and lysed in MPER (Thermo-Scientific, Erembodegem-Aalst, Belgium) supplemented with 1× protease inhibitor cocktail (Complete EDTA-free, Roche, Prohac, Luxembourg, Luxembourg) according to the manufacturer's instructions. Histones were isolated as previously reported.⁵⁴

Western blots were carried out as previously described.⁵⁵ Antibodies were from the following: from Sigma, anti-β-actin (A5441); from Santa Cruz Biotechnology (Heidelberg, Germany), antiacetylated α-tubulin (sc-23950), anti-SIRT1 (sc-15404), anti-SIRT2 (sc-20966); from Merck Millipore (Brussels, Belgium), anti-histone H1 (05-457), anti-histone H4 (05-858), anti-acetylated histone H4 (06-866), anti-acetylated histone H3 lysine 56 (04-1135); from Calbiochem, anti-tubulin (CP06); and the corresponding secondary antibody (all from Santa Cruz Biotechnology). β-Actin or α-tubulin and histone H1 or Coomassie blue staining (LKB, Villeneuve-la-Garenne, France) were used as loading controls for non-histone and histone proteins, respectively. Western blot membranes and Coomassie blue gels were quantified using ImageQuant TL (GE Healthcare, Roosendaal, The Netherlands) and ImageJ (U.S. National Institutes of Health, Bethesda, MD, USA) software, respectively, and data were reported to the control.

Statistical Analyses. Statistical analyses were carried out using the GraphPad Prism 6.0 software. One-way ANOVA and the Holm–Sidak multiple comparison tests were used for statistical comparisons. *p* values below 0.05 were considered as statistically significant.

■ ASSOCIATED CONTENT

Supporting Information

The Supporting Information is available free of charge on the ACS Publications website at DOI: 10.1021/acs.jmedchem.7b00533.

Additional experimental details; docking model of selected compounds in SIRT1 (PDB code 4ISI) and SIRT2 (PDB code 4RMG); in cellulo assessment of HDAC inhibition by compound **18** through the study of histone and α -tubulin acetylation levels; analysis of apoptosis induced by **18** in glioma cells; analysis of sub G1 population in glioblastoma cells treated with SIRTi; antitumor potential of compound **18**; summary of the IC₅₀ values obtained for compound **18** on various human cancer cell lines with acquired drug resistance; IC₅₀ values and biological data of newly described SIRT1 and/or SIRT2 inhibitors; supplementary references (PDF)
SMILES representations and some data (CSV)

■ AUTHOR INFORMATION

Corresponding Authors

*B.P. (chemistry): phone, + 32 4 366 43 65; fax, + 32 4 366 43 62; email, b.pirotte@ulg.ac.be.

*M.D.: (biology): phone, +82 2 880 8919; e-mail, marcdiederich@snu.ac.kr.

ORCID

Marc Diederich: 0000-0003-0115-4725

Notes

The authors declare no competing financial interest.

◆ M.S. and E.G. equally contributed to the work.

† B.P. and M.D. equally supervised the work.

■ ACKNOWLEDGMENTS

We gratefully thank Thierry Gras and Delphine Lamoral-Theys for their technical assistance. R.K. is a director of research with the Fonds National de la Recherche Scientifique (FRS-FNRS, Belgium). M.S. was supported by a “Waxweiler Grant for Cancer Prevention Research” from the Action Lions “Vaincre le Cancer”. LBMCC was supported by the “Recherche Cancer et Sang” foundation, by the “Recherches Scientifiques Luxembourg” association, by the “Een Häerz fir kriibskrank Kanner” association, by the Action LIONS “Vaincre le Cancer” association, and by Télévie Luxembourg. College of Pharmacy, SNU is supported by the NRF by the MEST of Korea for Tumor Microenvironment GCRC Grant 2012-0001184 and by Brain Korea (BK21) PLUS program.

■ ABBREVIATIONS USED

GG, global growth; HDAC, histone deacetylase; MDR, multi-drug resistance; MRP1, multidrug resistance protein 1; PBMC, peripheral blood mononuclear cell; PDB, Protein Data Bank; SA- β -gal, senescence-associated β -galactosidase; SAHA, suberoylanilide hydroxamic acid; SIRT, sirtuin; SIRTi, sirtuin inhibitor

■ REFERENCES

- (1) Lefranc, F.; Brotchi, J.; Kiss, R. Possible future issues in the treatment of glioblastomas: Special emphasis on cell migration and the resistance of migrating glioblastoma cells to apoptosis. *J. Clin. Oncol.* **2005**, *23*, 2411–2422.
- (2) Stupp, R.; Hegi, M. E.; Mason, W. P.; van den Bent, M. J.; Taphoorn, M. J.; Janzer, R. C.; Ludwin, S. K.; Allgeier, A.; Fisher, B.; Belanger, K.; Hau, P.; Brandes, A. A.; Gijtenbeek, J.; Marosi, C.; Vecht, C. J.; Mokhtari, K.; Wesseling, P.; Villa, S.; Eisenhauer, E.; Gorlia, T.;

Weller, M.; Lacombe, D.; Cairncross, J. G.; Mirimanoff, R. O. Effects of radiotherapy with concomitant and adjuvant temozolomide versus radiotherapy alone on survival in glioblastoma in a randomised phase iii study: 5-year analysis of the eortc-ncic trial. *Lancet Oncol.* **2009**, *10*, 459–466.

- (3) Cuperlovic-Culf, M.; Touaibia, M.; St-Coeur, P. D.; Poitras, J.; Morin, P.; Culf, A. S. Metabolic effects of known and novel hdac and sirt inhibitors in glioblastomas independently or combined with temozolomide. *Metabolites* **2014**, *4*, 807–830.

- (4) Folmer, F.; Orlikova, B.; Schneckeburger, M.; Dicato, M.; Diederich, M. Naturally occurring regulators of histone acetylation/deacetylation. *Curr. Nutr. Food Sci.* **2010**, *6*, 78–99.

- (5) Seidel, C.; Schneckeburger, M.; Dicato, M.; Diederich, M. Histone deacetylase modulators provided by mother nature. *Genes Nutr.* **2012**, *7*, 357–367.

- (6) Schneckeburger, M.; Florean, C.; Dicato, M.; Diederich, M. Epigenetic alterations as a universal feature of cancer hallmarks and a promising target for personalized treatments. *Curr. Top. Med. Chem.* **2016**, *16*, 745–776.

- (7) Seidel, C.; Florean, C.; Schneckeburger, M.; Dicato, M.; Diederich, M. Chromatin-modifying agents in anti-cancer therapy. *Biochimie* **2012**, *94*, 2264–2279.

- (8) Mei, Z.; Zhang, X.; Yi, J.; Huang, J.; He, J.; Tao, Y. Sirtuins in metabolism, DNA repair and cancer. *J. Exp. Clin. Cancer Res.* **2016**, *35*, 182.

- (9) Carafa, V.; Rotili, D.; Forgione, M.; Cuomo, F.; Serrettiello, E.; Hailu, G. S.; Jarho, E.; Lahtela-Kakkonen, M.; Mai, A.; Altucci, L. Sirtuin functions and modulation: From chemistry to the clinic. *Clin. Epigenet.* **2016**, *8*, 61.

- (10) Peck, B.; Chen, C. Y.; Ho, K. K.; Di Fruscia, P.; Myatt, S. S.; Coombes, R. C.; Fuchter, M. J.; Hsiao, C. D.; Lam, E. W. Sirt inhibitors induce cell death and p53 acetylation through targeting both sirt1 and sirt2. *Mol. Cancer Ther.* **2010**, *9*, 844–855.

- (11) Sakkiah, S.; Arooj, M.; Kumar, M. R.; Eom, S. H.; Lee, K. W. Identification of inhibitor binding site in human sirtuin 2 using molecular docking and dynamics simulations. *PLoS One* **2013**, *8*, e51429.

- (12) Trapp, J.; Jochum, A.; Meier, R.; Saunders, L.; Marshall, B.; Kunick, C.; Verdin, E.; Goekjian, P.; Sippl, W.; Jung, M. Adenosine mimetics as inhibitors of nad⁺-dependent histone deacetylases, from kinase to sirtuin inhibition. *J. Med. Chem.* **2006**, *49*, 7307–7316.

- (13) Medda, F.; Russell, R. J.; Higgins, M.; McCarthy, A. R.; Campbell, J.; Slawin, A. M.; Lane, D. P.; Lain, S.; Westwood, N. J. Novel cambinol analogs as sirtuin inhibitors: Synthesis, biological evaluation, and rationalization of activity. *J. Med. Chem.* **2009**, *52*, 2673–2682.

- (14) Outeiro, T. F.; Kontopoulos, E.; Altmann, S. M.; Kufareva, I.; Strathearn, K. E.; Amore, A. M.; Volk, C. B.; Maxwell, M. M.; Rochet, J. C.; McLean, P. J.; Young, A. B.; Abagyan, R.; Feany, M. B.; Hyman, B. T.; Kazantsev, A. G. Sirtuin 2 inhibitors rescue alpha-synuclein-mediated toxicity in models of Parkinson's disease. *Science* **2007**, *317*, 516–519.

- (15) Kim, H. W.; Kim, S. A.; Ahn, S. G. Sirtuin inhibitors, ex527 and agk2, suppress cell migration by inhibiting hsf1 protein stability. *Oncol. Rep.* **2016**, *35*, 235–242.

- (16) Florence, X.; Dilly, S.; de Tullio, P.; Pirotte, B.; Lebrun, P. Modulation of the 6-position of benzopyran derivatives and inhibitory effects on the insulin releasing process. *Bioorg. Med. Chem.* **2011**, *19*, 3919–3928.

- (17) Khelili, S.; Florence, X.; Bouhadja, M.; Abdelaziz, S.; Mechouch, N.; Mohamed, Y.; de Tullio, P.; Lebrun, P.; Pirotte, B. Synthesis and activity on rat aorta rings and rat pancreatic beta-cells of ring-opened analogues of benzopyran-type potassium channel activators. *Bioorg. Med. Chem.* **2008**, *16*, 6124–6130.

- (18) Ma, L.; Maruwge, W.; Strambi, A.; D'Arcy, P.; Pellegrini, P.; Kis, L.; de Milito, A.; Lain, S.; Brodin, B. Sirt1 and sirt2 inhibition impairs pediatric soft tissue sarcoma growth. *Cell Death Dis.* **2014**, *5*, e1483.

- (19) Trott, O.; Olson, A. J. Autodock vina: Improving the speed and accuracy of docking with a new scoring function, efficient optimization, and multithreading. *J. Comput. Chem.* **2010**, *31*, 455–461.

- (20) Rumpf, T.; Schiedel, M.; Karaman, B.; Roessler, C.; North, B. J.; Lehotzky, A.; Olah, J.; Ladwein, K. I.; Schmidtkunz, K.; Gajer, M.; Pannek, M.; Steegborn, C.; Sinclair, D. A.; Gerhardt, S.; Ovadi, J.; Schutkowski, M.; Sippl, W.; Einsle, O.; Jung, M. Selective sirt2 inhibition by ligand-induced rearrangement of the active site. *Nat. Commun.* **2015**, *6*, 6263.
- (21) Moniot, S.; Schutkowski, M.; Steegborn, C. Crystal structure analysis of human sirt2 and its adp-ribose complex. *J. Struct. Biol.* **2013**, *182*, 136–143.
- (22) Finnin, M. S.; Donigian, J. R.; Pavletich, N. P. Structure of the histone deacetylase sirt2. *Nat. Struct. Biol.* **2001**, *8*, 621–625.
- (23) Schiedel, M.; Rumpf, T.; Karaman, B.; Lehotzky, A.; Olah, J.; Gerhardt, S.; Ovadi, J.; Sippl, W.; Einsle, O.; Jung, M. Aminothiazoles as potent and selective sirt2 inhibitors: A structure-activity relationship study. *J. Med. Chem.* **2016**, *59*, 1599–1612.
- (24) Davenport, A. M.; Huber, F. M.; Hoelz, A. Structural and functional analysis of human sirt1. *J. Mol. Biol.* **2014**, *426*, 526–541.
- (25) Dai, H.; Case, A. W.; Riera, T. V.; Considine, T.; Lee, J. E.; Hamuro, Y.; Zhao, H.; Jiang, Y.; Sweitzer, S. M.; Pietrak, B.; Schwartz, B.; Blum, C. A.; Disch, J. S.; Caldwell, R.; Szczepankiewicz, B.; Oalman, C.; Yee Ng, P.; White, B. H.; Casaubon, R.; Narayan, R.; Koppetsch, K.; Bourbonais, F.; Wu, B.; Wang, J.; Qian, D.; Jiang, F.; Mao, C.; Wang, M.; Hu, E.; Wu, J. C.; Perni, R. B.; Vlasuk, G. P.; Ellis, J. L. Crystallographic structure of a small molecule sirt1 activator-enzyme complex. *Nat. Commun.* **2015**, *6*, 7645.
- (26) Cao, D.; Wang, M.; Qiu, X.; Liu, D.; Jiang, H.; Yang, N.; Xu, R. M. Structural basis for allosteric, substrate-dependent stimulation of sirt1 activity by resveratrol. *Genes Dev.* **2015**, *29*, 1316–1325.
- (27) Zhao, X.; Allison, D.; Condon, B.; Zhang, F.; Gheyi, T.; Zhang, A.; Ashok, S.; Russell, M.; MacEwan, I.; Qian, Y.; Jamison, J. A.; Luz, J. G. The 2.5 Å crystal structure of the sirt1 catalytic domain bound to nicotinamide adenine dinucleotide (nad⁺) and an indole (ex527 analogue) reveals a novel mechanism of histone deacetylase inhibition. *J. Med. Chem.* **2013**, *56*, 963–969.
- (28) Sayd, S.; Thirant, C.; El-Habr, E. A.; Lipecka, J.; Dubois, L. G.; Bogeas, A.; Tahiri-Jouti, N.; Chneiweiss, H.; Junier, M. P. Sirtuin-2 activity is required for glioma stem cell proliferation arrest but not necrosis induced by resveratrol. *Stem Cell Rev.* **2014**, *10*, 103–113.
- (29) Seidel, C.; Schnekenburger, M.; Dicato, M.; Diederich, M. Histone deacetylase 6 in health and disease. *Epigenomics* **2015**, *7*, 103–118.
- (30) Lefranc, F.; Nuzzo, G.; Hamdy, N. A.; Fakhr, I.; Moreno Y Banuls, L.; Van Goietsenoven, G.; Villani, G.; Mathieu, V.; van Soest, R.; Kiss, R.; Ciavatta, M. L. In vitro pharmacological and toxicological effects of norterpene peroxides isolated from the red sea sponge diacarnus erythraeanus on normal and cancer cells. *J. Nat. Prod.* **2013**, *76*, 1541–1547.
- (31) Branle, F.; Lefranc, F.; Camby, I.; Jeuken, J.; Geurts-Moespot, A.; Sprenger, S.; Sweep, F.; Kiss, R.; Salmon, I. Evaluation of the efficiency of chemotherapy in vivo orthotopic models of human glioma cells with and without 1p19q deletions and in c6 rat orthotopic allografts serving for the evaluation of surgery combined with chemotherapy. *Cancer* **2002**, *95*, 641–655.
- (32) Grandjenette, C.; Schnekenburger, M.; Karius, T.; Ghelfi, J.; Gaigneaux, A.; Henry, E.; Dicato, M.; Diederich, M. 5-aza-2'-deoxycytidine-mediated c-myc down-regulation triggers telomere-dependent senescence by regulating human telomerase reverse transcriptase in chronic myeloid leukemia. *Neoplasia* **2014**, *16*, 511–528.
- (33) Wang, X.; Simpson, E. R.; Brown, K. A. P53: Protection against tumor growth beyond effects on cell cycle and apoptosis. *Cancer Res.* **2015**, *75*, 5001–5007.
- (34) Gottesman, M. M.; Fojo, T.; Bates, S. E. Multidrug resistance in cancer: Role of atp-dependent transporters. *Nat. Rev. Cancer* **2002**, *2*, 48–58.
- (35) Yen, Y.; Grill, S. P.; Dutschman, G. E.; Chang, C. N.; Zhou, B. S.; Cheng, Y. C. Characterization of a hydroxyurea-resistant human kb cell line with supersensitivity to 6-thioguanine. *Cancer Res.* **1994**, *54*, 3686–3691.
- (36) Schuttelkopf, A. W.; van Aalten, D. M. Prodrig: A tool for high-throughput crystallography of protein-ligand complexes. *Acta Crystallogr., Sect. D: Biol. Crystallogr.* **2004**, *60*, 1355–1363.
- (37) Laskowski, R. A.; Swindells, M. B. Ligplot+: Multiple ligand-protein interaction diagrams for drug discovery. *J. Chem. Inf. Model.* **2011**, *51*, 2778–2786.
- (38) Le Mercier, M.; Fortin, S.; Mathieu, V.; Roland, I.; Spiegl-Kreinecker, S.; Haibe-Kains, B.; Bontempi, G.; Decaestecker, C.; Berger, W.; Lefranc, F.; Kiss, R. Galectin 1 proangiogenic and promigratory effects in the hs683 oligodendroglioma model are partly mediated through the control of bex2 expression. *Neoplasia* **2009**, *11*, 485–496.
- (39) Torsvik, A.; Stieber, D.; Enger, P. O.; Golebiewska, A.; Molven, A.; Svendsen, A.; Westermarck, B.; Niclou, S. P.; Olsen, T. K.; Chekenya Enger, M.; Bjerkvig, R. U-251 revisited: Genetic drift and phenotypic consequences of long-term cultures of glioblastoma cells. *Cancer Med.* **2014**, *3*, 812–824.
- (40) Stein, G. H. T98g: An anchorage-independent human tumor cell line that exhibits stationary phase g1 arrest in vitro. *J. Cell. Physiol.* **1979**, *99*, 43–54.
- (41) Roninson, I. B.; Chin, J. E.; Choi, K. G.; Gros, P.; Housman, D. E.; Fojo, A.; Shen, D. W.; Gottesman, M. M.; Pastan, I. Isolation of human mdr DNA sequences amplified in multidrug-resistant kb carcinoma cells. *Proc. Natl. Acad. Sci. U. S. A.* **1986**, *83*, 4538–4542.
- (42) Bunz, F.; Dutriaux, A.; Lengauer, C.; Waldman, T.; Zhou, S.; Brown, J. P.; Sedivy, J. M.; Kinzler, K. W.; Vogelstein, B. Requirement for p53 and p21 to sustain g2 arrest after DNA damage. *Science* **1998**, *282*, 1497–1501.
- (43) Schuurhuis, G. J.; Broxterman, H. J.; de Lange, J. H.; Pinedo, H. M.; van Heijningen, T. H.; Kuiper, C. M.; Scheffer, G. L.; Scheper, R. J.; van Kalken, C. K.; Baak, J. P.; Lankelma, J. Early multidrug resistance, defined by changes in intracellular doxorubicin distribution, independent of p-glycoprotein. *Br. J. Cancer* **1991**, *64*, 857–861.
- (44) Schnekenburger, M.; Grandjenette, C.; Ghelfi, J.; Karius, T.; Foliguet, B.; Dicato, M.; Diederich, M. Sustained exposure to the DNA demethylating agent, 2'-deoxy-5-azacytidine, leads to apoptotic cell death in chronic myeloid leukemia by promoting differentiation, senescence, and autophagy. *Biochem. Pharmacol.* **2011**, *81*, 364–378.
- (45) Goffin, E.; Lamoral-Theys, D.; Tajeddine, N.; de Tullio, P.; Mondin, L.; Lefranc, F.; Gailly, P.; Rogister, B.; Kiss, R.; Pirotte, B. N-aryl-n'-(chroman-4-yl)ureas and thioureas display in vitro anticancer activity and selectivity on apoptosis-resistant glioblastoma cells: Screening, synthesis of simplified derivatives, and structure-activity relationship analysis. *Eur. J. Med. Chem.* **2012**, *54*, 834–844.
- (46) Frederick, R.; Bruyere, C.; Vancraeynest, C.; Reniers, J.; Meinguet, C.; Pochet, L.; Backlund, A.; Masereel, B.; Kiss, R.; Wouters, J. Novel trisubstituted harmine derivatives with original in vitro anticancer activity. *J. Med. Chem.* **2012**, *55*, 6489–6501.
- (47) Mathieu, V.; Chantome, A.; Lefranc, F.; Cimmino, A.; Miklos, W.; Paulitschke, V.; Mohr, T.; Maddau, L.; Kornienko, A.; Berger, W.; Vandier, C.; Evidente, A.; Delpire, E.; Kiss, R. Sphaeropsidin A shows promising activity against drug-resistant cancer cells by targeting regulatory volume increase. *Cell. Mol. Life Sci.* **2015**, *72*, 3731–3746.
- (48) Mathieu, V.; Van Den Berge, E.; Ceusters, J.; Konopka, T.; Cops, A.; Bruyere, C.; Pirker, C.; Berger, W.; Trieu-Van, T.; Serteyn, D.; Kiss, R.; Robiette, R. New 5-aryl-1h-imidazoles display in vitro antitumor activity against apoptosis-resistant cancer models, including melanomas, through mitochondrial targeting. *J. Med. Chem.* **2013**, *56*, 6626–6637.
- (49) Seidel, C.; Schnekenburger, M.; Mazumder, A.; Teiten, M. H.; Kirsch, G.; Dicato, M.; Diederich, M. 4-hydroxybenzoic acid derivatives as hdac6-specific inhibitors modulating microtubular structure and hsp90alpha chaperone activity against prostate cancer. *Biochem. Pharmacol.* **2016**, *99*, 31–52.
- (50) Piccinini, F.; Tesei, A.; Arienti, C.; Bevilacqua, A. Cancer multicellular spheroids: Volume assessment from a single 2d projection. *Comput. Methods Programs Biomed.* **2015**, *118*, 95–106.
- (51) Florean, C.; Schnekenburger, M.; Lee, J. Y.; Kim, K. R.; Mazumder, A.; Song, S.; Kim, J. M.; Grandjenette, C.; Kim, J. G.; Yoon, A. Y.; Dicato, M.; Kim, K. W.; Christov, C.; Han, B. W.; Proksch, P.; Diederich, M. Discovery and characterization of isofistularin-3, a marine

brominated alkaloid, as a new DNA demethylating agent inducing cell cycle arrest and sensitization to trail in cancer cells. *Oncotarget* **2016**, *7*, 24027–24049.

(52) El Amrani, M.; Lai, D.; Debbab, A.; Aly, A. H.; Siems, K.; Seidel, C.; Schnekenburger, M.; Gaigneaux, A.; Diederich, M.; Feger, D.; Lin, W.; Proksch, P. Protein kinase and hdac inhibitors from the endophytic fungus *epicoccum nigrum*. *J. Nat. Prod.* **2014**, *77*, 49–56.

(53) Seidel, C.; Schnekenburger, M.; Dicato, M.; Diederich, M. Antiproliferative and proapoptotic activities of 4-hydroxybenzoic acid-based inhibitors of histone deacetylases. *Cancer Lett.* **2014**, *343*, 134–146.

(54) Nunes, M. J.; Milagre, I.; Schnekenburger, M.; Gama, M. J.; Diederich, M.; Rodrigues, E. Sp proteins play a critical role in histone deacetylase inhibitor-mediated derepression of *cyp46a1* gene transcription. *J. Neurochem.* **2010**, *113*, 418–431.

(55) Karius, T.; Schnekenburger, M.; Ghelfi, J.; Walter, J.; Dicato, M.; Diederich, M. Reversible epigenetic fingerprint-mediated glutathione-S-transferase p1 gene silencing in human leukemia cell lines. *Biochem. Pharmacol.* **2011**, *81*, 1329–1342.

(56) Pirotte, B.; Florence, X.; Goffin, E.; Medeiros, M. B.; de Tullio, P.; Lebrun, P. 4-phenylureido/thioureido-substituted 2,2-dimethylchroman analogs of cromakalim bearing a bulky “carbamate” moiety at the 6-position as potent inhibitors of glucose-sensitive insulin secretion. *Eur. J. Med. Chem.* **2016**, *121*, 338–351.